POLITECNICO DI TORINO

Corso di Laurea Magistrale
in Ingegneria Aerospaziale

Tesi di Laurea Magistrale

IMPROVEMENT OF MAIN ROTOR MODEL FOR COMMERCIAL FULL FLIGHT HELICOPTER SIMULATOR

Relatore
prof. Giorgio Guglieri

Candidato
Lapo Pietrolati
matricola 266348

Relatore aziendale TXT e-solutions spa
ing. Matteo Righi

Marzo-2022

Summary

The main rotor model of an existing commercial Full Flight Simulator of a small twin-engine utility helicopter is improved. The existing rotor model implements individual rigid blades with flap blade dynamic in loose way causing an unstable flight dynamic and uncoupled off-axis response. The work aims to obtain a stable response of the flight model after the trim phase and an improved dynamic response more comparable to the flight tests data to reduce the artificial tuning phase. Furthermore, to maintain high general configurability and to respect the real-time simulation constrain a special attention is given to the practical implementation of the code.

To solve the instability problem a multi-blade coordinates transformation of the existing model is introduced. Additionally, to improve output stability, the rotor model is transformed to be non-rotating and, therefore, independent from the time discretization. The multiblade coordinates transformation acts as a low pass filter in the time integration without any loss of accuracy and any extra hypothesis, permitting to naturally increase stability in a discrete time model. Stopping the rotation of the blades leads to time independent eigenvalues of the system increasing the output stability. The consequent loss of accuracy is partially reestablished by artificially increasing the number of blades and then mediating the output for the real number of rotor blades. This artifice can be performed only with the multi-blade coordinates transformation.

The nonexistence of an off-axis response in many flight situations has imputed to the poor quality of the main rotor model. A higher level rotor model is developed and implemented, maintaining the multi-blade coordinates transformation and the time independency artifice. The new model has individual rigid blades featuring flap and lag blade dynamics around offsetted concentrated hinges, a 3 state dynamic inflow model, a non-linear 2D blade aerodynamic and numerical integrated aerodynamic loads. The equations are evaluated without performing any further simplification with Matlab symbolic tool and the implementation scheme is reorganized to maintain higher level of generality.

Contents

List of Figures

List of Tables

List of Symbols

A_{1s}	cyclic roll command	[rad]
B_{1c}	cyclic pitch command	[rad]
L	Transformation matrix	
$M_{a\,\beta}$	Blade aerodynamic moment about the flap hinge	[Nm]
$M_{a\,\zeta}$	Blade aerodynamic moment about the lag hinge	[Nm]
Q	Required shaft torque	[Nm]
R	Rotation matrix	
U_p	Perpendicular velocity at blade element	[m/s]
U_r	Radial velocity at blade element	[m/s]
U_t	Tangential velocity at blade element	[m/s]
V	Flow velocity at blade element	[m/s]
α	Angle of attack	[rad]
β_w	Hub-wind rotation angle	[rad]
$\lambda_0\,,\ \lambda_{1s}\,, \lambda_{1c}$	Inflow states	[−]
ρ	Atmospheric density	[Kg/m^3]
θ_0	collective command	[rad]
θ_G	Geometrical pitch	[rad]
θ_{twist}	Geometrical twist	[rad]
φ	Inflow angle	[rad]
$\vec{F}$	Force vector	[N]
$\vec{M}$	Moment vector	[Nm]

$\vec{M}_{disk\,H}$	Moment vector of the inflow model	[Nm]
$\vec{U}_{inflow}$	Inflow velocity vector	[m/s]
$\vec{V}$	Linear velocity vector	[m/s]
$\vec{\omega}$	Angular velocity vector	[rad/s]
$e\vec{c}c$, ecc	Real or equivalent hinge offset: eccentricity. Vector and scalar value	[m]
$\vec{r}$, r	Blade element location from hinge. Vector and scalar value	[m]
$\vec{r}_{BH}$	Hub position vector from GC	[m]
$\vec{r}_{Rb}$	Vector blade element location from hub centre	[m]
a	Linear acceleration component	[m/s]
c_b	blade chord of generic blade element	[m]
c_s	Speed of sound	[m/s]
c_β	Flap hinge dumping	[Nms/Rad]
c_ζ	Lag hinge dumping	[Nms/Rad]
i_ψ, i_θ	lateral and longitudinal shaft tilt angles	[rad]
k_β	Flap equivalent concentrated hinge stiffness	[Nm/Rad]
k_ζ	Lag equivalent concentrated hinge stiffness	[Nm/Rad]
p	Body pitch velocity	[rad/s]
q	Body roll velocity	[rad/s]
r	Body yaw velocity	[rad/s]
u	Longitudinal velocity	[m/s]
v	Lateral velocity	[m/s]
w	Vertical velocity	[m/s]
x_B, y_B, z_B	Body frame of reference, coordinate axis	
x_H, y_H, z_H	Fixed hub frame of reference, coordinate axis. Hub position coordinates in body reference frame	
x_R, y_R, z_R	Rotating hub frame of reference, coordinate axis	
x_b, y_b, z_b	blade frame of reference, coordinate axis	
C_D	Drag coefficient	[−]

C_L	Lift coefficient	[–]
$C_{F\,a}$	Aerodynamic force coefficient	[–]
C_T	Trust coefficient, TPP coordinate system	[–]
C_l	Roll moment coefficient, TPP coordinate system	[–]
C_m	Pitch moment coefficient, TPP coordinate system	[–]
L	Roll moment, TPP coordinate system	[Nm]
M	Pitch moment, TPP coordinate system	[–]
M	Pitch moment, TPP coordinate system	[Nm]
N	Number of rotor blades	
T	Trust, TPP coordinate system	[N]
β_0	Flap degree of freedom, multiblade coordinates: coning	[rad]
β_{0d}	Flap degree of freedom, multiblade coordinates: differential mode	[rad]
β_{nc}	Flap degree of freedom, multiblade coordinates: cosine cyclic	[rad]
β_{ns}	Flap degree of freedom, multiblade coordinates: sine cyclic	[rad]
$\nu_0\,,\,\nu_{nc}\,,\nu_{ns}\,,\nu_{0d}\,,$	Generic b^{th} blade degree of freedom, multiblade coordinates	
$\nu_{(b)}$	Generic blade degree of freedom, individual blade coordinates	
$\psi\,,\,\psi_b,\,\psi_{(b)}$	Blade azimuth position	[rad]
$\psi\,,\,\theta\,,\,\phi$	Euler angles	[rad]
ζ_0	Lead-lag degree of freedom, multiblade coordinates: coning	[rad]
ζ_{0d}	Lead-lag degree of freedom, multiblade coordinates: differential mode	[rad]
ζ_{nc}	Lead-lag degree of freedom, multiblade coordinates: cosine cyclic	[rad]
ζ_{ns}	Lead-lag degree of freedom, multiblade coordinates: sine cyclic	[rad]
n	Cyclic modal number, multiblade coordinates	
n_r	Number of rotor blade multiples	
$t\,,\,\Delta t$	Time, discrete time step	[s]
β	Blade flap angle (positive: blade up)	[rad]
ζ	Blade lead-lag angle (positive: blade forward)	[rad]

Chapter 1

The existing simulator

1.1 Introduction

Flight simulation has gained great importance in the latest decades, especially in the pilot training field. Modern full flight simulators must ensure a high level of fidelity, fundamental to train pilots for both conventional and emergency flight situations. In particular, it has proved to be of great importance in training helicopter pilots for flight situations or operations that are potentially dangerous for both pilots and people on the ground, and as well for the machine itself.
Greater accuracy and better and more faithful modeling of the characteristic phenomena of flight allow pilots to be trained with greater harmony with the machine and with greater fidelity to the behavior of the aircraft throughout the flight envelope. Furthermore, they allows to create, validate and certify a flight simulator more efficiently.
The most significant element that affects the flight dynamic of the helicopter surely is the main rotor, therefore an intense effort must be devoted to model this component. Many different degrees of rotor complexity can be achieved in modeling; however, the accuracy should be consistently defined within the application area, the imposed objectives and the constraints, as well as balanced with the other subsystem models.

For a FFS, the objective of the model is to ensure consistency and accuracy of the flight dynamics and performance compared to the simulated helicopter, for the whole flight envelope and even for the emergency maneuvers (auto-rotation, icing, etc.). First of all, a very complex and highly detailed model requires long computational time that can not be performed in a real-time simulation. Furthermore, many complex phenomenal that affect the rotor or the individual blades are only minimally responsible of the overall flight response, hence the uselessness of an over-complex model for the training simulation field. On the other hand, a simplistic model would require extensive and complex tuning, proving to be expensive, inflexible, hardly configurable and mostly unreliable at the limits of flight envelopes.
One of the most important imposed constrain of the project is the configurability and generality of the simulator. The aim is to be able to simulate a large variety of helicopter

of similar category by changing configurations and parameters. To obtain such capability from the code, it is necessary to perform an adequate physical modelling of all the components, considering also a certain level of modularity of the implementation of the model and its phisical components. Given the fact that many different technical solution for rotor heads are usually employed, from a fully hinged to a bearingless one, the rotor model should be able to simulate most of those, by activating the proper dedicated sub-module and/or by shaping a very general one.

My work has been done on an existing commercial code of an helicopter simulator that is in development. After the my internship at the TXT e-solutions with the team that was developing the simulator it has been proposed to me to work on the improvement of the main rotor model, as a master thesis work. When the thesis started, the simulator was already working but the main motor model module was still in a early development stage.
The simulated helicopter is a light utility twin engine. The first part of the work is carried out on a four-blade hingeless helicopter; the second one is developed on a different helicopter, one with a 5-blade bearingless main rotor with elastic flap-lag-pitch hinges.
Both helicopter simulators will be certified as full flight simulator. Validation of the models are performed over a vast database of flight test data and with a vast use of the QTG, also in the inital development stages [1].
Many parameters of the design of the rotor are obtained from the flight manuals, meanwhile some specific parameters are estimated by comparing available data with the literature of similar helicopters.

1.2 Current model: feature, problems and limitations

The originally implemented rotor model features a only-flapping individual blade dynamic, with perfectly rigid blades flapping about an equivalent hinge with offset. Blade aerodynamic is CFD evaluated, 2D non linear, steady and with compressibility effects up to M=0.8. Polar extrapolation to 360° angle of attack is performed over the computed CL-CD data. Aerodynamic loads are evaluated with a numeric left-rule Riemann sum (rectangles) on a coarse blade discretization. A tip loss factor is used to correct the contribution of the tip aerodynamic load by restricting the integration domain. Inflow model is based on the Pitt/Peters[13] first harmonic 3 dof. Ground effect and ice effect are modelled with simple correction gains. Stand-alone wake model is implemented but not yet activated; it is designed to only correct aerodynamic loads of tail surfaces in forward flight. No aerodynamic blade-blade or blade-body interaction is modelled. Inertial

[1] QTG: Qualification Test Guide.
The QTG is the primary reference document used for evaluating an FSTD. It contains test results, statements of compliance and other information for the evaluator to assess if the FSTD meets the test criteria described in this AMC.[3]

loads contribution is evaluated only to adjust the flapping stiffness for the flapping blade dynamic. No inertial force and moments are transferred to the helicopter through the shaft.
The general assumptions on which the model is based are summarized below:

- Blade dynamic: rigid blades, 3dof flap about the offsetted hinge.
- Blade aerodynamic: 2D non linear, steady, compressibility, numerically integrated loads.
- Inflow: Pitt/Peters first harmonic inflow model, 3 dof dynamic inflow (non-uniform)[13].

Problems and limitations

At the time of starting this thesis work, the development team highlighted some issues related to the main rotor model code. Two major flight dynamic issues were found:

- Unstable flight dynamic following some maneuver.
- Wrong but mostly nonexistent off-axis (or cross-coupling) dynamic response.

Along with some dynamic flight tests, the simulated helicopter response becomes unstable and slowly diverging, unlike the real helicopter which remains stable. Instability problems are mainly ascribable to numerical integration effects ans numerical errors, therefore some kind of filter should be used.

Commonly, a helicopter responds to a single-axis control input with multi-axis behaviour - quoting Padfield [12]: «cross-coupling is almost synonymous with helicopters». However, the simulation results are not completely in line with the expected ones, showing an unstable dynamic and the nonexistence of the off-axis (or cross-coupling) response. To obtain a correct off-axis response, a review of the simplifications and approximations must be performed and a more rigorous model scheme must be implemented.

Some other "secondary" issues are also found and an attempt has been made to resolve them in this work.

- "Stiff" implementation: high complexity to expand the model or to add higher level submodules.
- Neglected inertial loads: loss of important contribution to the flight dynamic.
- Equations with high level of approximation and linearization performed with insufficient rigorousness and presenting many neglected therms.
- Non physical parameters: the main rotor parameters (such as blade inertia, blade mass, equivalent spring hinge stiffness and eccentricity) are set with very different values from real helicopter in order to obtain a comparable flight behaviour.
- Coefficient-based equations: incoherence in the normalization (normalization or adimensionalization occur with different reference values), almost doubled calculations, numerical errors.

- Model implementation appears to be not well conditioned.

Extensive and complex artificial tuning is necessary to obtain the accuracy requested from a FFS certification from the current model. Implementation of the original model is not well structured to satisfy the demanded level of configurability and generality.

1.3 Improvement methods

Accordingly with the previously highlighted problems, this thesis aimed to improve the previous work by augmenting the level of solutions and the degree of complexity, both in the modelling and the implementation. First of all, the instability problem is solved by employing the multiblade coordinates transformation over the existing model: in fact it acts like a low pass filter without modifying the model accuracy, such as described in part I. In the second an the third steps of model development, such as described in part II, a complete new model is evaluated and implemented to solve the off-axis dynamic behaviour problems and to build a much rigorous, configurable and even efficient code.

Part I

Improvement of existing rotor model

Chapter 2

Multi-blade coordinate transformation

2.1 Theory

Main rotor models equipped with such a level of accuracy necessary for full flight simulators are generally expressed as rotating frames attached to the individual blades. The main rotor responds as a whole to excitations that mostly occurs in a nonrotating frame: as a matter of fact, the rotor system sees the combined effect of all blades. Multi-blade coordinate transformation properly models the dynamic interaction between the nonrotating fuselage and the spinning rotor, helping to integrate the dynamic of individual blades and expressing the combined effect in the non rotating frame. An helicopter main rotor is a periodic system, which blade equations usually contains all harmonics. MBC transformation highlight the filtering behaviour of a rotor that allows only specific blade motion harmonics to be seen from rest of the fixed system. MBC transformation filters out exactly all the unnecessary periodic therms that are not integral multiples of ΩN, where Ω is the rotor angular speed and N is the number of rotor blades. This filtering action also makes the system equations numerically well-conditioned [4].

With the MBC, it was possible to increase the output model stability by averaging over the rotor rotational period without omitting all periodic terms that contribute to the system dynamics. To do this, the rotation of the rotor is kept fixed for each discretization time step of the simulation. Errors due to the time discretization of the rotation of the fixed rotor are increased. To partially recover the ability of the rotor to capture phenomena affecting the blades in different azimuth positions, a n_r multiple of blades have been added. For the MBC transformation, to be correctly applicable, the blades must be equally spaced around the azimuth. The overall output of the rotor is therefore averaged over the n_r number of rotors.

Analysing a rotor with N equally spaced blades around the azimuth ψ, each one located at ψ_b from the azimuth reference location, is possible to introduce the transformation from individual coordinates (IBCs) to multiblade coordinates (MBCs) [2]. For the helicopter

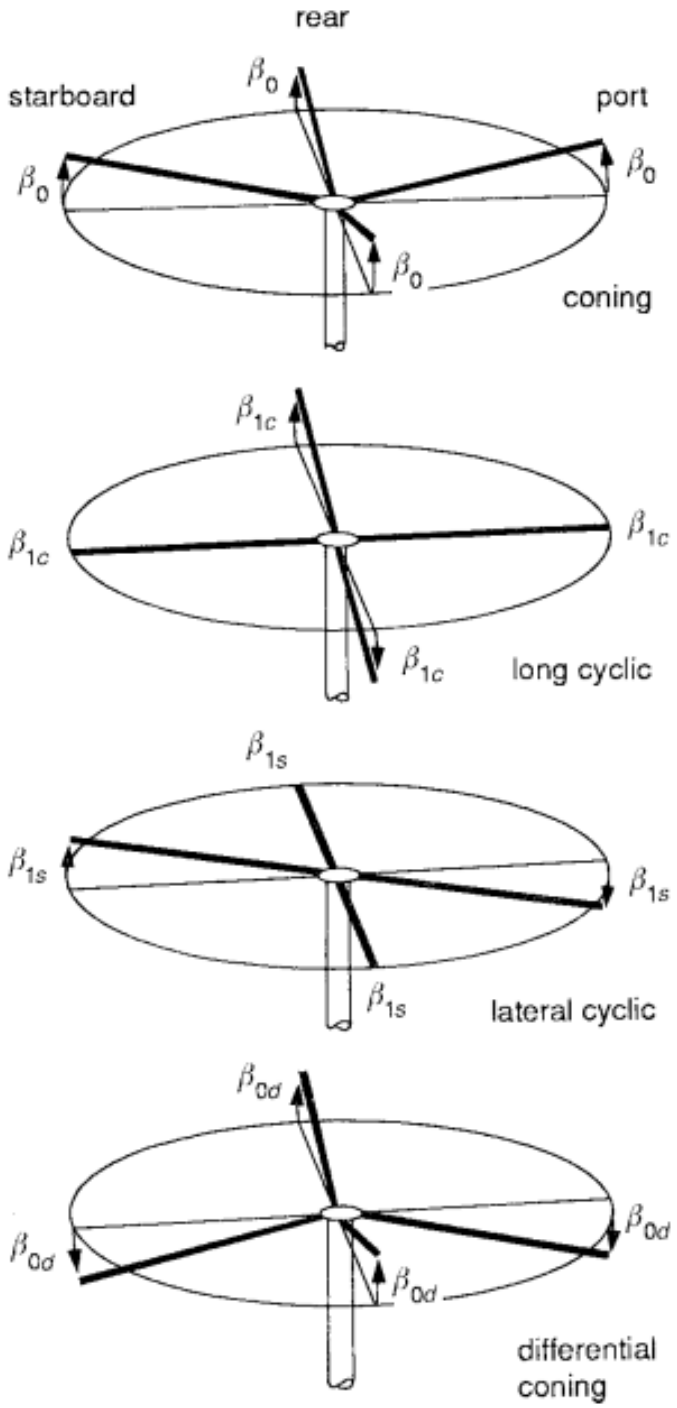

Figure 2.1. Multiblade flapping physical representation

main rotor the zero-azimuth reference is the one pointing to the rear of the fuselage, so the first blade location is $\psi_0 = 0$, but for a rotating rotor this can be evaluated as $\psi_0 = \Omega t$ where t is continuous or discrete time. The blade azimuth can be generically defined by the relation:

$$\psi_b = \Omega t + (b-1)\frac{2\pi}{N} \tag{2.1}$$

The relations for the transformation from IBCs to MBCs are expressed for blade generic degree of freedom ν_b:

$$\nu_0 = \frac{1}{N}\sum_{b=1}^{N}\nu_b \tag{2.2}$$

$$\nu_{nc} = \frac{2}{N}\sum_{b=1}^{N}\nu_b cos(n\psi_b) \tag{2.3}$$

$$\nu_{ns} = \frac{2}{N}\sum_{b=1}^{N}\nu_b sin(n\psi_b) \tag{2.4}$$

$$\nu_{0d} = \frac{1}{N}\sum_{b=1}^{N}\nu_b(-1)^b \tag{2.5}$$

Physical interpretation of the multiblade coordinates can be easily done for the flapping degree of freedom $\nu = \beta$ as shown in Figure: 2.1, where: β_0 is the coning angle, β_{1c} and β_{1s} are the cosine-cyclic and sine-cyclic modes, that from a tip path-plane point of view represent respectively the fore-aft tilt and the side-side tilt of the rotor TPP. The β_{nc} and β_{ns} with $n > 1$ are called reactionless modes, because they do not cause any transfer of loads from the rotor to the helicopter (hub fixed frame). The last therm β_{0d} is called differential mode and it is present only when N is even. The cyclic modal number n goes from 1 to $(N-1)/2$ if N is odd or from 1 to $(N-2)/2$ if N is even. An equally simple physical interpretation can be used for the lead-lag degree of freedom ζ. Replacing ν_b with ζ_b, where ζ_b is the individual blade lead-lag angle, therefore ζ_0 becomes the rotor lag angle; ζ_{1c} and ζ_{1s} represent respectively the longitudinal shift and the lateral shift of rotor center of mass.

Inverse transformation from MBCs to IBCs is also fundamental for the implementation scheme and it is expressed as follows for the generic degree of freedom ν_b of the b-th blade:

$$\nu_b = \nu_0 + \sum_n(\nu_{nc}cos(n\psi_b) + \nu_{ns}sin(n\psi_b)) + \nu_{0d}(-1)^b \tag{2.6}$$

2.2 Implementation

Implementation of the multiblade transformation is performed by creating a code wrap around the main rotor model module, in order to continue to use the original main rotor model. Flapping angular velocity and angular accelerations that are evaluated in the individual blade frame are transformed in multiblade coordinates and injected into the numerical time integrator, in order to evaluate the model states at the next time step. An

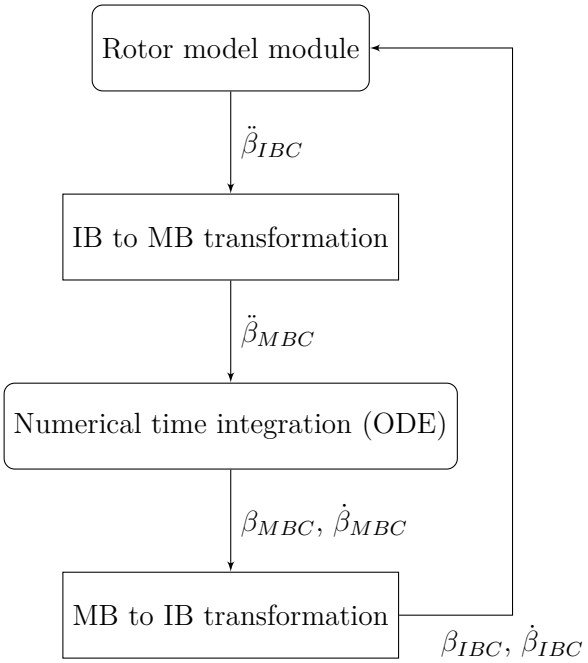

Table 2.1. Multiblade implementation

inverse transformation from MBC to IBC is performed on the resulting blade states: flap angle and angular velocity, in order to use them coherently in the main rotor module, as shown in the table 2.1. MBC transformation does not degrade the output of the model dynamic, therefore the number of the states remains as in the old model; however, it is the physical interpretation of those states that has changed. The states in the old model stand for the flap angle and for the angular velocity for each blade; the new MBC transformed states, instead, represents, as mentioned before, the whole rotor behaviour. Therefore, nothing has changed also in the numerical integration (ODE) module.

Since the main rotor model describes the blade flapping dynamic with a second order model implemented as two states variable, it is necessary to evaluate the direct and inverse transformation for the appropriate flapping derivative order. For sake of clarity, the implemented transformations formula are expressed:

- IBCs to MBCs transformation of $\ddot{\beta}$

$$\ddot{\beta}_0 = \frac{1}{N}\sum_{b=1}^{N}\ddot{\beta}_b \tag{2.7}$$

$$\ddot{\beta}_{nc} = \frac{2}{N}\sum_{b=1}^{N}\left(\ddot{\beta}_b cos(n\psi_b) - 2nsin(n\psi_b)\dot{\beta}_b\Omega - nsin(n\psi_b)\beta_b\dot{\Omega} - n^2 cos(n\psi_b)\beta_b\Omega^2\right) \tag{2.8}$$

$$\ddot{\beta}_{ns} = \frac{2}{N}\sum_{b=1}^{N}\left(\ddot{\beta}_b sin(n\psi_b) + 2ncos(n\psi_b)\dot{\beta}_b\Omega + ncos(n\psi_b)\beta_b\dot{\Omega} - n^2 sin(n\psi_b)\beta_b\Omega^2\right). \tag{2.9}$$

$$\ddot{\beta}_{0d} = \frac{1}{N}\sum_{b=1}^{N}\left(\ddot{\beta}_b(-1)^b\right). \tag{2.10}$$

- MBCs to IBCs inverse transformation of β and $\dot{\beta}$.

$$\beta_b = \beta_0 + \sum_n(\beta_{nc}cos(n\psi_b) + \beta_{ns}sin(n\psi_b)) + \beta_{0d}(-1)^b \tag{2.11}$$

$$\begin{aligned}\dot{\beta}_b =& \dot{\beta}_0 + \sum_n\left(\dot{\beta}_{nc}cos(n\psi_b) + \dot{\beta}_{ns}sin(n\psi_b) + (cos(n\psi_b)\beta_{ns} - sin(n\psi_b)\beta_{nc})n\Omega\right) + \\ &+ \dot{\beta}_{0d}(-1)^b.\end{aligned} \tag{2.12}$$

2.2.1 Averaging and stopping rotation

To further improve the stability of the dynamic response of the rotor model, the artifice of blocking the rotation and averaging the output over a large number of blades (or number of overlapping rotors) has been exploited. To stop the rotor rotation, the azimuth position of the blades is no longer updated based on the frame time integration, and the blades are always considered in the same position. The first term of the equation (2.1) is always zero.

This artifice resolves the instabilities and divergences of the simulated dynamic but it degrades the level of generality of the model. In this way, the contribution of the single blade is not evaluated when it is in a position different than the one imposed. To partially recover generality and refine the "discretization" on the blade lap, the number of equally spaced blades is increased. Therefore, the output of forces and moments at the hub is averaged on the basis of the real number of blades of the simulated helicopter. The theoretical implications of this solution have not been sufficiently explored in this study but the consistency of the results obtained with respect to the flight test data guided the choice. In literature a similar approach is commonly used in order to time-average the periodic state-space matrix over the rotor rotational period, and then to apply conventional eigenanalysis to compute modal and stability characteristics. Furthermore, it must

follow MBC to not erase all periodic terms that contribute to the dynamics of the system causing erroneous results [5] [9].

Code implementation aimed to obtain highest level of efficiency for the real-time computation. Therefore, some code improvements have been made during the implementation of the MBCs. The trim convergence logic has been enhanced, allowing a visible improvement in model performance, even if the calculated number of blades is quadrupled.

It is also interesting to clarify of how the trim analysis is performed by the code. To solve the trim analysis mathematically, it is necessary to find the minimum of a set of nonlinear equations within defined constraints. The code solves the trim analysis through a zero-finding numerical iterative method. For each iteration step, the problem is divided in two sub-steps: at first, it is computed the only-rotor trim (called steady state trim) and then it is computed the rotor-plus-fuselage trim (and all the other helicopter components). The steady state trim computation is performed by minimizing, within certain tolerances, only the rotor states derivatives (also called residuals) by varying the values of the rotor states. The initial guesses of those states are automatically selected depending on the flight trim condition. Once the steady state achieves convergence, the problem is expanded with the rest of the helicopter components. It is then evaluated the trim of all the system by also minimizing the other states derivatives within certain tolerances. The problem is solved when the states derivatives (residuals) have reached lower values than those of certain tolerances. This trim process takes 5-4 seconds and increases up to 6 seconds when the rotor output is averaged on a n_r of 8 blades multiples (hence 32 blades).

The use of MBCs in the code can be activated and deactivate simply via configuration switch.

Chapter 3

Test results

In this chapter we observe the simulator results comparing the same model with and without multi-blade coordinates.

The tests performed are based on data from real helicopter flight tests. All tests and data are obtained with the aim of validating the model and certifying the simulator, therefore they comply with the reference legislation standards[3].

The flight tests taken into consideration to compare the model with and without multi-blade coordinates are those of the static snapshot type. These flight tests observe for a certain period of time the dynamics of the helicopter with fixed commands for particular initial conditions (i.e. trim condition).

For the snapshot tests the initial reference conditions are calculated as an average value over the measured data history, with the exception of mass properties and environmental parameters.

If the dynamic of the helicopter in the observed attitude condition is stable, the time evolution of the simulated helicopter state should remain stationary. In the case of the individual-blade coordinate model, some of these tests resulted to be unstable with divergent dynamics.

In the following results, some characteristic parameters of the aircraft dynamic are overplotted, comparing real data and the data of the two simulated models. The initial (or trim) parameters are also tabulated.

The simulated tests are operated by a dedicated tool/program, which also manages the validation of these tests and the generation of the documents necessary for certification (i.e. QTG and MQTG). These documents are also of fundamental importance for all stages of development and validation even outside the certification phase.

The tests reported for the validation of MBCs in this thesis are two and have been chosen among those from the old model that presented the major instability problems.

3.1 Test 1.g

This first test, called 1.g [3] version A2, observes the state of the helicopter in a flight condition which implies a positive climb rate of about $9.2 m/s$, forward speed of about

68.8kts and small sideslip angle of about 5deg. It is a flight situation that occurs easily during normal helicopter operational missions. All the initial data are reported in table 3.1; weight and balance information are also reported.

The blue plot line is the reference measured data, the purple line is the individual blade coordinate model and the staggered green plot is the multiblade coordinate model output.

Real helicopter measured data show stable behavior of the aircraft.

Observing the simulated flight tests of the individual blade coordinate model, there is a slight instability and divergence of almost all the flight data.

A notable divergence is observed from the temporal trend of the Euler angles i.e. bank, pitch and heading. Even if the instability of the dynamics appears to be slow and with a very little amplitude gain, it can be easily felt by test pilots, specially if it occurs in such standard flight condition, by remarkably increasing the pilot workload.

Flight test data always show noise and small vibrations that should not be taken into account for the comparison process.

Multiblade coordinate model does not shows any sign of divergence, keeping the output steady as desired.

Parameter [UoM]	Reference	FSTD	MQTG
Mass Properties			
Gross Weight [kg]	3360.6	3360.6	3360.6
Fuel Weight [kg]	545	545	545
CG Longitudinal [mm]	4398	4398	4398
CG Lateral [mm]	5	5	5
Moment of Inertia XX; XY; XZ [kgm^2]	4437; 29; -1656	3523; 13; -1750	3523; 13; -1750
Moment of Inertia YX; YY; YZ [kgm^2]	29; 16791; 11	13; 13102; 9	13; 13102; 9
Moment of Inertia ZX; ZY; ZZ [kgm^2]	-1656; 11; 19169	-1750; 9; 10945	-1750; 9; 10945
Environment Parameters			
Pressure Altitude [ft]	7961.9	7950.7	7950.9
OAT [degC]	15.3	15.2	15.2
Wind Direction [deg]	0	0	0
Wind Speed [kts]	0	0	0
Flight Parameters			
Airspeed [kts]	68.5	68.8	68.8
Ground Speed [kts]	70.8	79.4	79.3
Vertical Velocity [ft/min]	2074.5	1800	1820
Radar Altitude [ft]	915.4	8002.3	8003
Rotor Speed [%]	101.8	101.7	101.7
Engine 1 Torque [%]	94	90.6	91.5
Engine 2 Torque [%]	94.1	90.6	91.5
Pitch Angle [deg]	4.2	2.8	3
Bank Angle [deg]	-1.9	-2.7	-2.9
Heading [deg]	171.3	171.6	172
Pitch Rate [deg/s]	0.2	0	0.1
Roll Rate [deg/s]	-0.2	0	-0.1
Yaw Rate [deg/s]	-0.2	0	0.5
Sideslip Angle [deg]	5	5.2	4.6
X Body Acceleration [m/s^2]	-0.1	0	0
Y Body Acceleration [m/s^2]	0	0	0
Z Body Acceleration [m/s^2]	0	0	0
Longitudinal Cyclic Pos. [%]	35.8	37.1	37
Lateral Cyclic Pos. [%]	46.1	51.1	51.1
Pedals Pos. [%]	29.3	19.4	19.3
Collective Pos. [%]	74.4	50.9	51.3
Engine 1 Main Switch [-]	FLIGHT	FLIGHT	FLIGHT
Engine 2 Main Switch [-]	FLIGHT	FLIGHT	FLIGHT
AFCS State [-]	ATRIM	ATRIM	ATRIM

Table 3.1. 1.g A2 initial test data

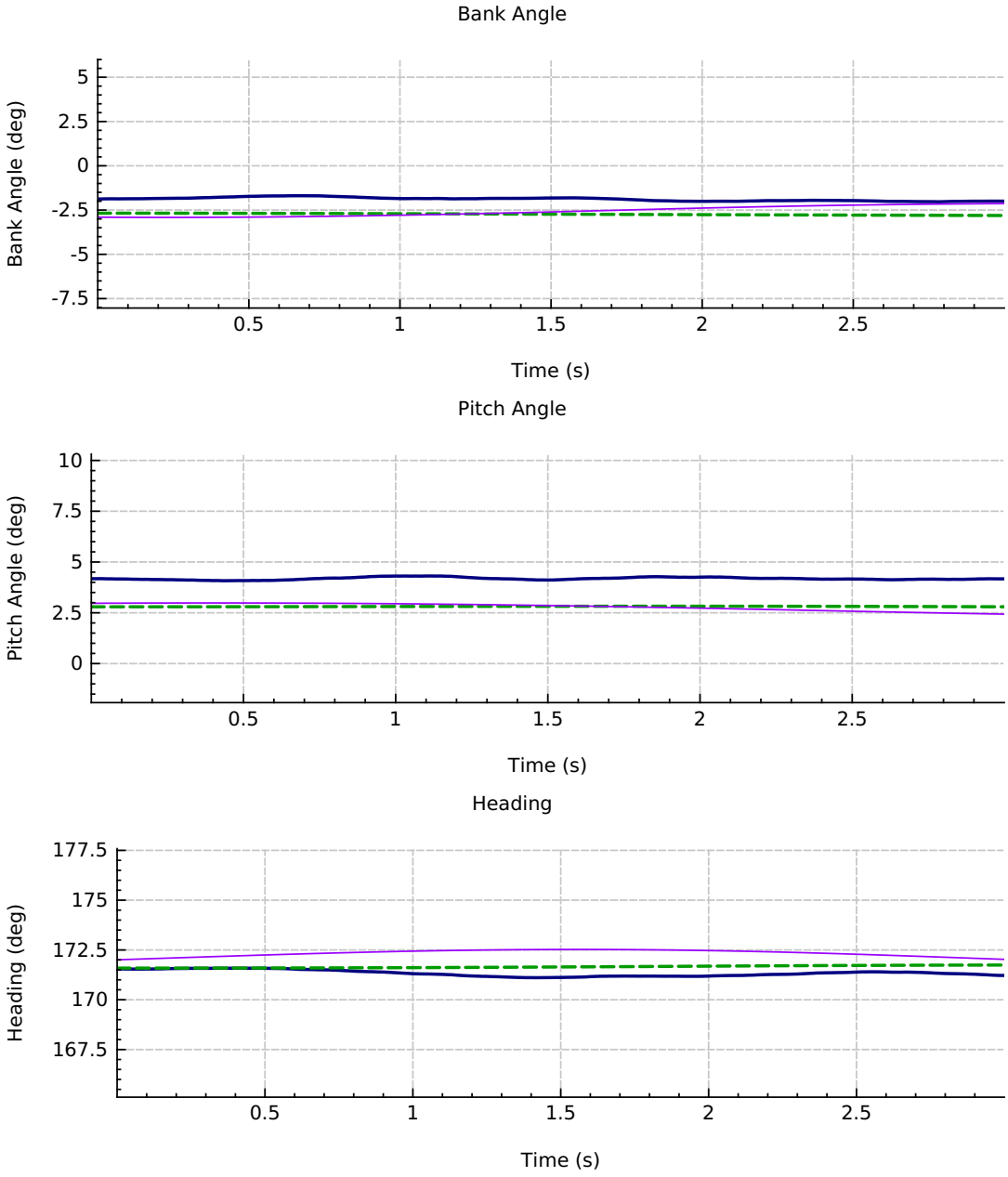
Bank Angle
Bank Angle (deg)
5
2.5
0
-2.5
-5
-7.5
0.5
1
1.5
2
2.5
Time (s)
Pitch Angle
Pitch Angle (deg)
10
7.5
5
2.5
0
0.5
1
1.5
2
2.5
Time (s)
Heading
Heading (deg)
177.5
175
172.5
170
167.5
0.5
1
1.5
2
2.5
Time (s)

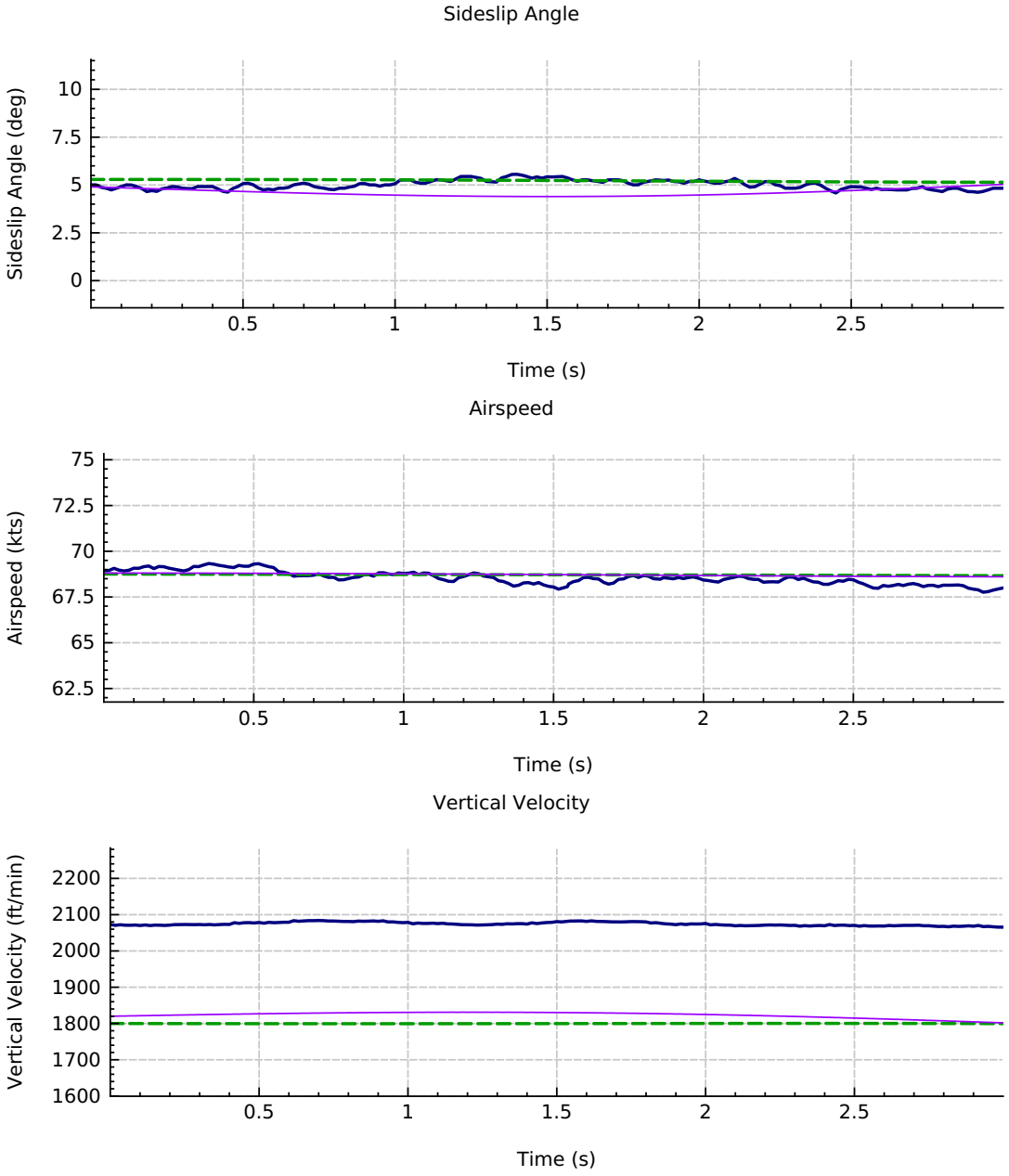
Sideslip Angle
Sideslip Angle (deg)
10
7.5
5
2.5
0
0.5
1
1.5
2
2.5
Time (s)
Airspeed
Airspeed (kts)
75
72.5
70
67.5
65
62.5
0.5
1
1.5
2
2.5
Time (s)
Vertical Velocity
Vertical Velocity (ft/min)
2200
2100
2000
1900
1800
1700
1600
0.5
1
1.5
2
2.5
Time (s)

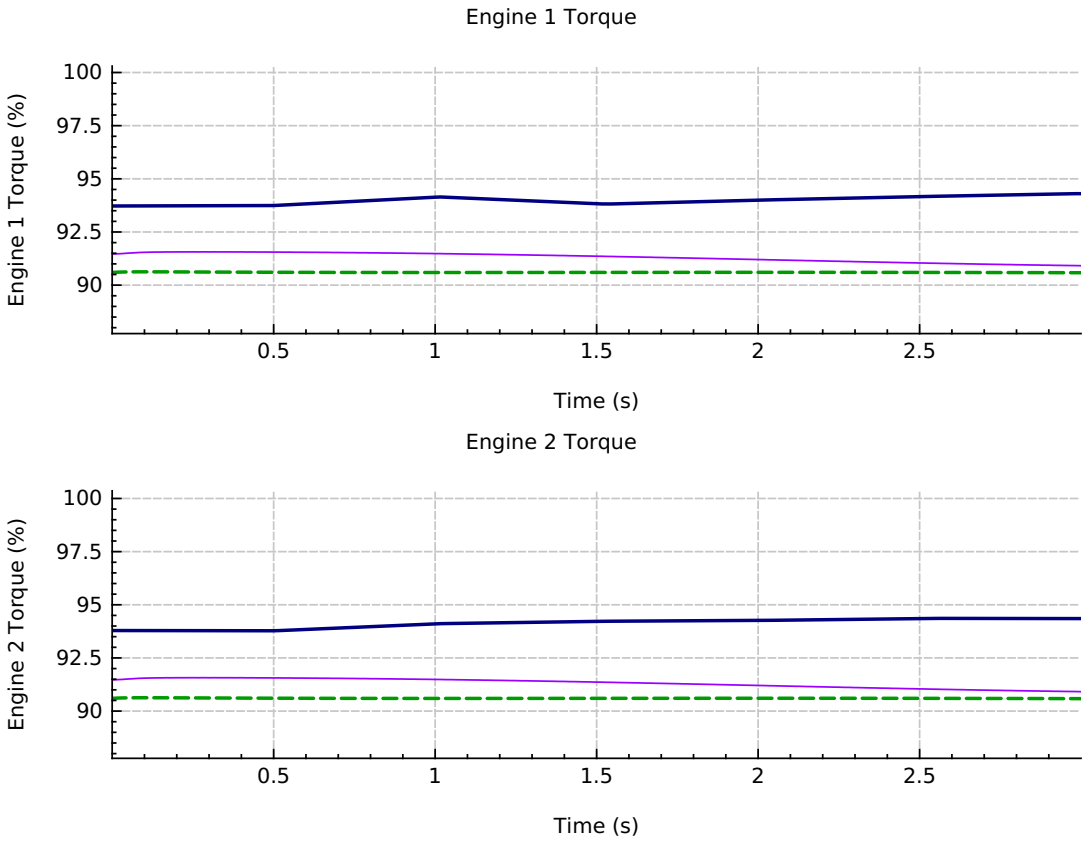

Figure 3.1. 1.g test results

3.2 Test 2.d.2

This second test, called 2.d.2 [3] version D3, observes the state of the helicopter in a flight condition with almost zero climb, forward airspeed of about $97kts$ and important sideslip angle of about $13deg$. It is a mid-high-speed flight situation with large sideslip angle, a flight condition with almost maximum sideslip angle that can be reached with such airspeed. All the initial data are reported in table 3.2, weight and balance information are also reported.
The blue plot line is the reference measured data, the purple line is the individual blade coordinate model and the staggered green plot is the multiblade coordinate model output. Real helicopter measured data show stable behavior of the aircraft also for this flight test. Observing the simulated flight tests of the individual blade coordinate model, it can bee seen a strong instability and severe divergence of all the flight data, as if the helicopter is entering a sort of dive spiraling flight. Multiblade coordinate model data show a huge improvement in simulation fidelity, keeping the output steady as desired.

If observing carefully, a beginning of slight dynamic divergence is also found for the multiblade coordinate model starting from the test time of $2.5s$ (in the Euler angles plot is much more evident).

This behaviour could be attributed to other components of the modelled helicopter. For such a sideslip angle and airspeed, the aerodynamic contribution of the helicopter body and tail surfaces is strongly affecting the aircraft flight dynamic. Therefore, it is necessary to investigate the contribution of the fuselage sub-models, vertical and horizontal tail plane and probably also of the tail rotor. It is also likely that the wake model needs to be improved for the corrections of the incident flow on the tail planes.

In conclusion, we can say that the results obtained with multiblade coordinates guarantee an important improvement of the model.

Parameter [UoM]	Reference	FSTD	MQTG
Mass Properties			
Gross Weight [kg]	3278.9	3278.9	3278.9
Fuel Weight [kg]	428	428	428
CG Longitudinal [mm]	4428	4428	4428
CG Lateral [mm]	2	2	2
Moment of Inertia XX; XY; XZ [kgm2]	4214; 14; -1587	3346; 25; -1719	3346; 25; -1719
Moment of Inertia YX; YY; YZ [kgm2]	14; 16327; 6	25; 12650; 11	25; 12650; 11
Moment of Inertia ZX; ZY; ZZ [kgm2]	-1587; 6; 18870	-1719; 11; 10667	-1719; 11; 10667
Environment Parameters			
Pressure Altitude [ft]	11134.3	11123.3	11123.5
OAT [degC]	-6.1	-6.1	-6.1
Wind Direction [deg]	0	0	0
Wind Speed [kts]	0	0	0
Flight Parameters			
Airspeed [kts]	97.2	97.2	96.5
Ground Speed [kts]	109.2	118.7	118.7
Vertical Velocity [ft/min]	-25.3	0.3	20.9
Radar Altitude [ft]	999.5	11134.6	11134.9
Rotor Speed [%]	103.6	103.5	103.5
Engine 1 Torque [%]	58.7	53.1	54.1
Engine 2 Torque [%]	58.7	53.1	54.1
Pitch Angle [deg]	-0.3	1.9	2.8
Bank Angle [deg]	-8.7	-13.4	-15.7
Heading [deg]	261	260.6	262.2
Pitch Rate [deg/s]	0	0	1.1
Roll Rate [deg/s]	-0.4	0	-4.9
Yaw Rate [deg/s]	-0.4	0	4.8
Sideslip Angle [deg]	-13	-13	-23
X Body Acceleration [m/s2]	0	0	0
Y Body Acceleration [m/s2]	-0.1	-0.2	-0.2
Z Body Acceleration [m/s2]	0	0	0
Longitudinal Cyclic Pos. [%]	38.1	36.7	36.4
Lateral Cyclic Pos. [%]	42.8	56.6	57
Pedals Pos. [%]	72.7	64.5	64.2
Collective Pos. [%]	58.4	31.6	32.5
Engine 1 Main Switch [-]	FLIGHT	FLIGHT	FLIGHT
Engine 2 Main Switch [-]	FLIGHT	FLIGHT	FLIGHT
AFCS State [-]	OFF	OFF	OFF

Table 3.2. 2.d.2 initial test data

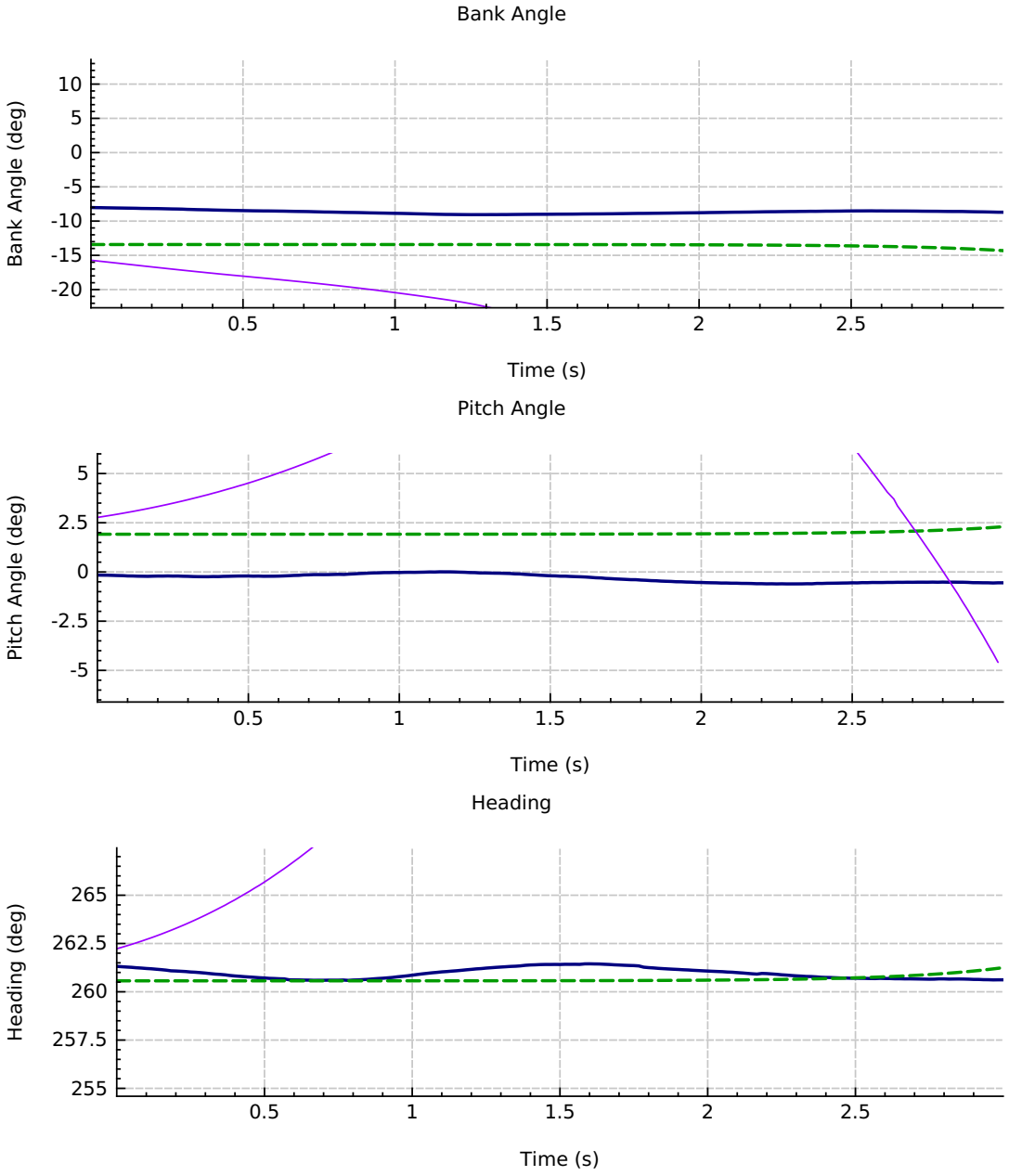
Bank Angle
Bank Angle (deg)
10
5
0
-5
-10
-15
-20
0.5
1
1.5
2
2.5
Time (s)
Pitch Angle
Pitch Angle (deg)
5
2.5
0
-2.5
-5
0.5
1
1.5
2
2.5
Time (s)
Heading
Heading (deg)
265
262.5
260
257.5
255
0.5
1
1.5
2
2.5
Time (s)

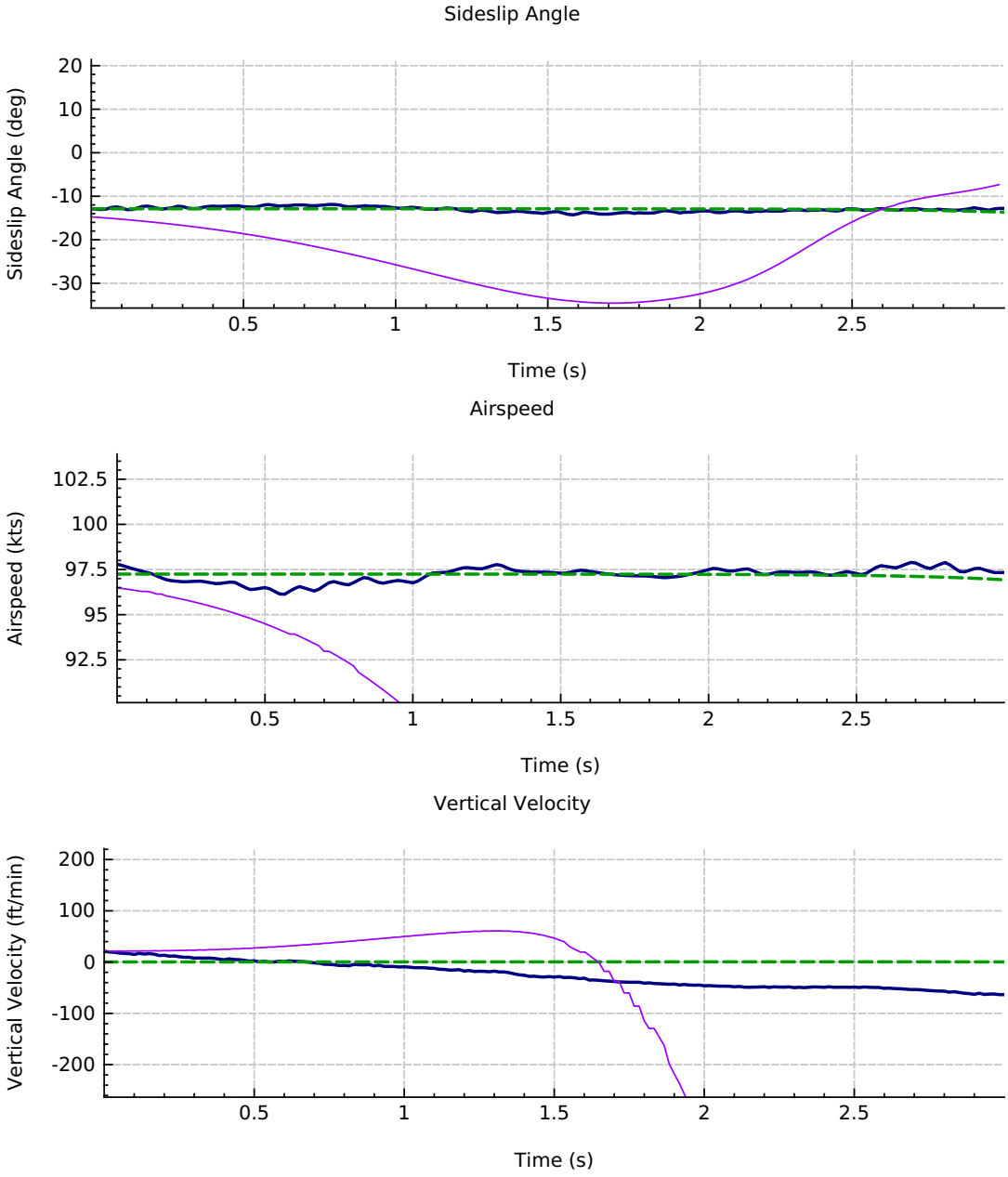
Sideslip Angle
Sideslip Angle (deg)
20
10
0
-10
-20
-30
0.5
1
1.5
2
2.5
Time (s)
Airspeed
Airspeed (kts)
102.5
100
97.5
95
92.5
0.5
1
1.5
2
2.5
Time (s)
Vertical Velocity
Vertical Velocity (ft/min)
200
100
0
-100
-200
0.5
1
1.5
2
2.5
Time (s)

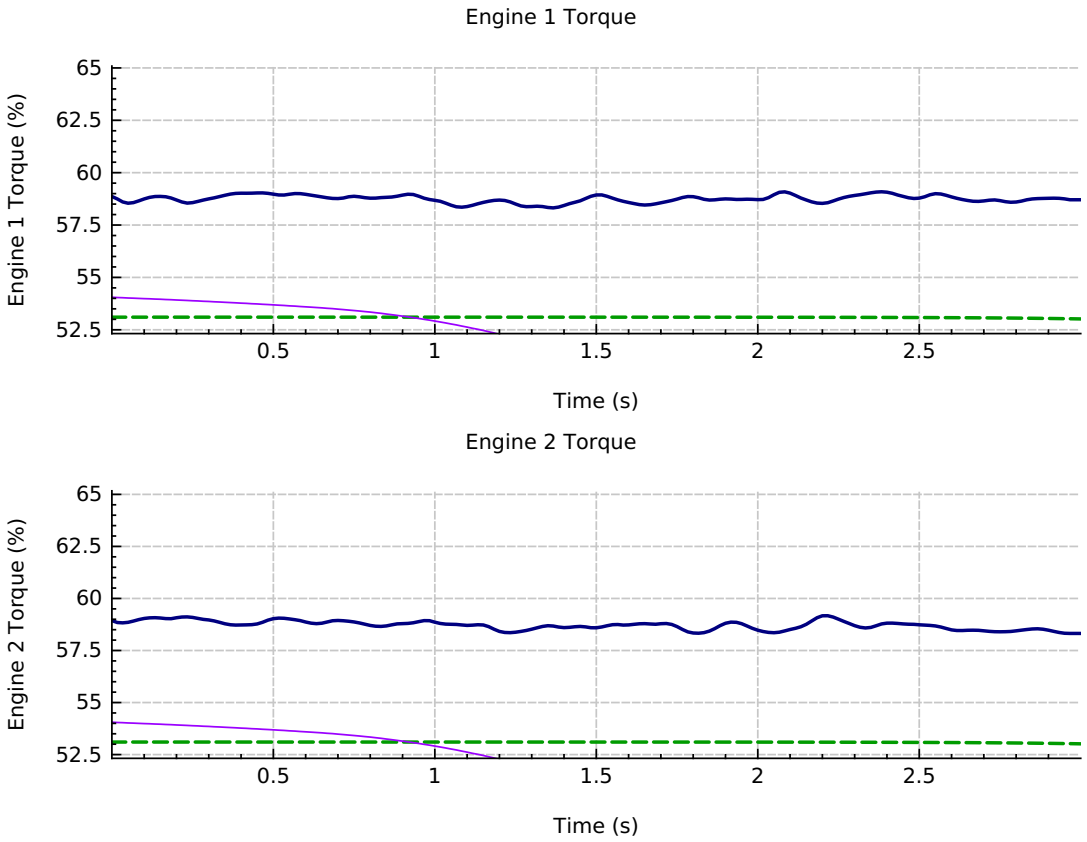

Figure 3.2. 2.d.2 test results

Part II

New model development and implementation

Chapter 4

New rotor model

With the work done with the multiblade coordinate implementation and other minor code cleaning, the main rotor model capability is still to be considered inadequate for the simulator. First of all, it does not solve the off-axis response problem, and on the second hand, but still important, none of the side issues cited in section 1.2 are addressed, except a slight code optimization.

The main task of this second part of the thesis work aims to level up the rotor modeling and to solve most of the side issues. The effort required for the development of a new model was assessed as necessary, and anyway smaller than modifying the old model.

In the making process, it was also involved the company purpose to develop a new, much robust, modular and general rotor model. Such model also should have been a starting point for future developments and improvements.

The new model design and formulation is inspired from the one described in the "UH-60A Black Hawk Engineering Simulation Program, Volume 1" [8] and in [14], that features a single main rotor with articulated blades. The main evolution from the old model is the insertion of the lead-lag degree of freedom. Hence, the blade dynamic is now described by a coupled flap-lead 6 degrees of freedom dynamic. As a matter of fact, the lag and flap degrees of freedom are strongly coupled: neglecting the lead-lag degree of freedom is a strong assumption [1] [9] [12]. However, to maximize modularity and configurability of the model, there is the possibility to turn off the lead-lag dofs or activate different sub-models.

The new model is developed and implemented in a more structured and rigorous manner. A good degree of configurability through physical parameters of the helicopter is aimed, trying to minimize the need for artificial tuning. Model equations are dimensional and no terms are neglected to maintain higher level of generality; more, it appears to define a better-conditioned model. Some equation therms contribution is negligible for this helicopter or for the most of the flight envelope, but it is not certain that it is also negligible for other helicopters or out of the flight envelope.

The intricate equations that result are evaluated by intense usage of a Matlab® symbolic script[10] that was developed to evaluate the complete equations of the main rotor

model in the most generic way.

The general assumptions on which the model is based are summarized below:

- Blade dynamic: rigid blades, 6dof flap lead-lag, about concentrated offsetted hinge.
- Blade aerodynamic: 2D non linear, steady, compressibility, numerically integrated loads.
- Inflow: Pitt/Peters first harmonic inflow model: 3 dof dynamic inflow (non-uniform)[13].

The blade is modelled as rigid with the mass concentrated along the span axis (y_b), which is also the point of application of the forces. Blade flap and lead dynamic occur about a offsetted hinge. This level of blade modelling is extensively used in both hingeless and hinged rotors. By the way, to model blade as elastic it is required a profound knowledge of the blade structure, limiting the ease of configurability and generality of the model. The flap and lag stiffness are thus modelled with equivalent hinge-concentrated springs.

Blade aerodynamic is defined as in the original model. However, aerodynamic loads are now evaluated with numerical integration by trapezoidal rule. The blade discretization is parametric and configurable by the number of elements and by the element size stretching through exponential trend. Integration domain can be limited to neglect 3D aerodynamic effect of root and tip effects.

The multiblade coordinate transformation is employed as in the first part of this work, maintaining the stopping of the rotor rotation and the averaging over a multiple number of blades. Also the sub-models of inflow and wake are kept the same as in the original model.

The computation scheme and implementation have been thoroughly revisited taking into account the need to improve computation performance and code rigorousness. The implementation of the model was also carried out, trying to maintain a good degree of the code understanding for any future development.

The work was carried out by following steps. At first, the new model with only active flap dynamics was validated, then the lag dynamics was activated and at the end the influence of the parameters was evaluated.

4.1 Theory

In this section, there are summarized all the main rotor model hypothesis, the model input and the model output.

General model hypothesis can be listed:

1. Articulated rotor with flap β and lead-lag ζ blades dynamic.
2. Rigid blade, with mass concentrated along the blade span.
3. Blade flap and lead-lag occurs about coincident hinge, offsetted from the shaft.

4. Blade weight is neglected in the model equations.
5. Blade aerodynamic loads are evaluated with blade element theory.
6. Blade element aerodynamic is 2D, steady, compressibility.
7. Pitching moment of blade element is neglected.
8. Aerodynamic loads are numerically integrated.
9. 3-dof unsteady and non uniform inflow model. Pitt/Peters [13]
10. Concentrated springs and dampers in the blade hinge to model blade stiffness for bearingless or hingeless rotor heads and lag damper devices.

The hypothesis implications on the model are discussed in the next chapters, along with the formulations.

Input and Output of the model

In order to insert the new rotor model alongside the old one in the same code structure, input and output must be consistent. Output and input are listed:

Main rotor module model input:

- helicopter linear and angular velocity and accelerations in body reference frames: $\vec{V}_B$, $\vec{\omega}_B$, $\dot{\vec{V}}_B$, $\dot{\vec{\omega}}_B$.
- rotor rotation speed and acceleration Ω, $\dot{\Omega}$.
- main rotor commands: θ_0, A_{1s}, B_{1c}.
- inflow states: λ_0, λ_{1s}, λ_{1c}.
- rotor states (multiblade coordinates): β, $\dot{\beta}$, ζ, $\dot{\zeta}$.
- rotor configuration data.
- atmospheric data.
- aerodynamic 2D tables.

Main rotor module model output:

- rotor states derivatives (multiblade coordinates): $\dot{\beta}$, $\ddot{\beta}$, $\dot{\zeta}$, $\ddot{\zeta}$
- inflow states derivatives: $\dot{\lambda}_0$, $\dot{\lambda}_{1s}$, $\dot{\lambda}_{1c}$.
- forces and moments (body frame of reference) $\vec{F}_B$, $\vec{M}_B$
- required shaft torque Q.

4.1.1 Frames of reference

For the development of the main rotor equations, the following reference frames are used:

- Body reference frame, with the origin at the centre of gravity of the helicopter.
- Fixed hub reference frame, with the origin at the hub centre.
- Rotating hub reference frames, with the same origin of the fixed hub frame, rotating with the rotor head.
- Blade reference frames, with the origin at the blade hinge.
- Blade element reference frames, with the origin along the blade span axis.

To maintain the highest level of generality, the rotation matrices are generated by the conventional fixed-to-rotating transformation of frames of references by adequate definition of Euler angles sets. Where the first rotation occurs about the yaw axis, the second occurs about the pitch axis and the last one occurs about the roll axis, as described in the appendix A. The rotation angles set is represented here by a vector that contains the angles of rotation in the correct order.

Non rotating frames

Body fixed frame is centered into the centre of gravity of the helicopter.
Hub fixed frame is centered at the centre of the rotor disk, shifted by $\vec{r}_{BH} = \begin{pmatrix} x_H & y_H & z_H \end{pmatrix}'$ from the body frame origin[1]. The shaft is tilted aft by an angle i_θ and to the right by i_ϕ, thus making its z axis coincident with the main rotor shaft as described in Figure 4.1. Body to fixed hub rotation matrix is computed by the angles rotation sequence: $\begin{pmatrix} i_\phi & i_\theta & 0 \end{pmatrix}$.

$$L_{B2H} = \begin{bmatrix} \cos(i_\theta) & 0 & -\sin(i_\theta) \\ \sin(i_\phi)\sin(i_\theta) & \cos(i_\phi) & \cos(i_\theta)\sin(i_\phi) \\ \cos(i_\phi)\sin(i_\theta) & -\sin(i_\phi) & \cos(i_\phi)\cos(i_\theta) \end{bmatrix} \tag{4.1}$$

[1] B subscript is used to refer quantities to the body frames and H subscript for the hub frame.

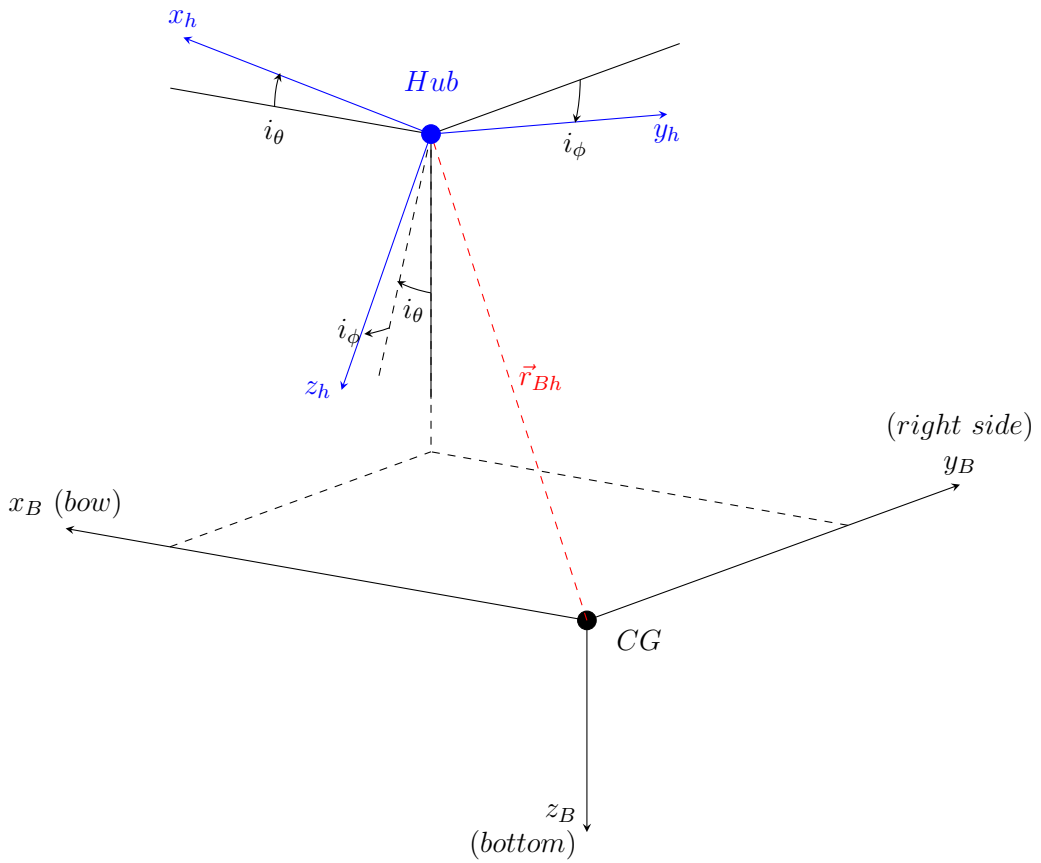

Figure 4.1. Body and fixed hub reference frames

Rotating frames, blade frames

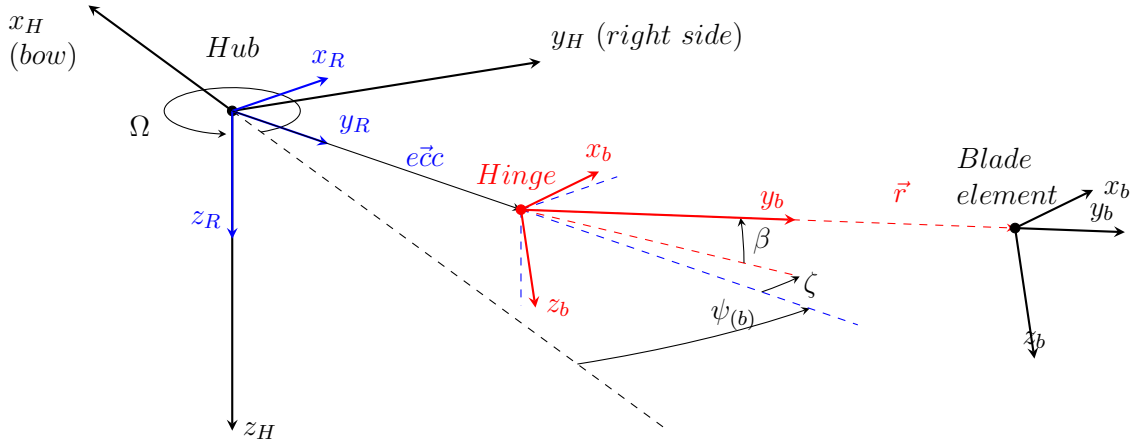

Figure 4.2. Hub fixed reference frame, Hub Rotating reference frame and blade reference frame

The rotating reference frames is constrained to the rotating hub of the main rotor and it y_R is aligned with the b-th blade eccentricity arm, and it also shares with the non rotating frame the same origin at the centre of the disk rotor.
Hub fixed to hub rotating transformation matrix is computed by the rotation sequence: $\begin{pmatrix} 0 & 0 & -\psi_{(b)} + \pi/2 \end{pmatrix}$.[2]

Where $\psi_{(b)}$ refers to the b^{th} blade azimuth location.

$$L_{H2R} = \begin{bmatrix} \sin(\psi) & \cos(\psi) & 0 \\ -\cos(\psi) & \sin(\psi) & 0 \\ 0 & 0 & 1 \end{bmatrix} \tag{4.2}$$

The other rotating reference frame, called blade reference frame, is integral with the b^{th} rigid blade and it is centered at the blade flap-lead hinge. It is shifted by the vector $e\vec{c}c = \begin{pmatrix} 0 & ecc & 0 \end{pmatrix}^T$ in the rotating coordinate frame. Hub Rotating to blade frame transformation matrix is computed by the rotation sequence: $\begin{pmatrix} -\beta & 0 & -\zeta \end{pmatrix}$

Where β refers to the b^{th} blade flapping angle and ζ refers to the b^{th} blade leading angle.

[2]From now on, the (b) subscription of the parameters referred to the b^{th} blade is omitted in all the right side of the explicit formulation of this discussion and it is used only when a misunderstanding could occur.

$$L_{R2b} = \begin{bmatrix} \cos(\zeta) & -\sin(\zeta) & 0 \\ \cos(\beta)\,\sin(\zeta) & \cos(\beta)\,\cos(\zeta) & -\sin(\beta) \\ \sin(\beta)\,\sin(\zeta) & \sin(\beta)\,\cos(\zeta) & \cos(\beta) \end{bmatrix} \tag{4.3}$$

Blade element reference frame

Blade span axis (y_b) is the location where the blade mass is distributed and where the aerodynamic forces act. Therefore, the so called blade element reference frame represents the blade section location at a distance r from the hinge and along the y_b axis. The focus of the blade section, i.e. the 25% or airfoil chord, lies on the origin of the latter reference system with the l.e. pointing towards the positive x_b axis, as can be seen in figure 4.4. Blade span location of blade element in blade reference frame is given by the vector $\vec{r} = \begin{pmatrix} 0 & r & 0 \end{pmatrix}^T$.

4.1.2 Equation of motion

To evaluate the blade element velocity and accelerations, it is necessary to transform the helicopter kinematic data referred to the body frame to the proper rotor frames of references. The first step requires to transform the linear and angular velocity from body to non-rotating Hub reference frame.

Input linear and angular velocity (body) are defined from the following vectors:

$$\vec{V}_B = \begin{pmatrix} u_B & v_B & w_B \end{pmatrix}^T \tag{4.4}$$

$$\vec{\omega}_B = \begin{pmatrix} p_B & q_B & r_B \end{pmatrix}^T \tag{4.5}$$

The fixed hub velocity is evaluated by applying the appropriate transformation matrix:

$$\vec{V}_H = L_{B2H}\left(\vec{V}_B + \vec{\omega}_B \times \vec{r}_{BH}\right) \tag{4.6}$$

$$\vec{\omega}_H = L_{B2H}\,\vec{\omega}_B \tag{4.7}$$

The resulting equation sets are made explicit:

$$\vec{V}_H = \begin{pmatrix} \cos(i_\theta)\,(u_B - y_h\,r_B + z_h\,q_B) - \sin(i_\theta)\,(w_B - x_h\,q_B + y_h\,p_B) \\ \cos(i_\phi)\,(v_B + x_h\,r_B - z_h\,p_B) + \cos(i_\theta)\,\sin(i_\phi)\,(w_B - x_h\,q_B + y_h\,p_B) + \\ \quad +\sin(i_\phi)\,\sin(i_\theta)\,(u_B - y_h\,r_B + z_h\,q_B) \\ \cos(i_\phi)\,\cos(i_\theta)\,(w_B - x_h\,q_B + y_h\,p_B) - \sin(i_\phi)\,(v_B + x_h\,r_B - z_h\,p_B) + \\ \quad +\cos(i_\phi)\,\sin(i_\theta)\,(u_B - y_h\,r_B + z_h\,q_B) \end{pmatrix} \tag{4.8}$$

$$\vec{\omega}_H = \begin{pmatrix} \cos(i_\theta)\ p_B(t) - \sin(i_\theta)\ r_B(t) \\ \cos(i_\phi)\ q_B(t) + \cos(i_\theta)\ \sin(i_\phi)\ r_B(t) + \sin(i_\phi)\ \sin(i_\theta)\ p_B(t) \\ \cos(i_\phi)\ \cos(i_\theta)\ r_B(t) - \sin(i_\phi)\ q_B(t) + \cos(i_\phi)\ \sin(i_\theta)\ p_B(t) \end{pmatrix} \tag{4.9}$$

Accelerations

Input linear and angular accelerations (body) are defined from the following vectors:

$$\vec{\dot{V}}_B = \begin{pmatrix} \dot{u}_B & \dot{v}_B & \dot{w}_B \end{pmatrix}^T \quad \vec{\dot{\omega}}_B = \begin{pmatrix} \dot{p}_B & \dot{q}_B & \dot{r}_B \end{pmatrix}^T \tag{4.10}$$

With the same matricial approach, the accelerations are evaluated at the fixed hub frame:

$$\vec{\dot{V}}_H = L_{B2H}\left(\vec{\dot{V}}_H + \vec{\dot{\omega}}_B \times \vec{r}_{BH} + \vec{\omega}_B \times (\vec{\omega}_B \times \vec{r}_{BH})\right) \tag{4.11}$$

$$\vec{\dot{\omega}}_H = L_{B2H}\,\vec{\dot{\omega}}_B \tag{4.12}$$

Explicit formulation for the latter set of equations is omitted.

4.1.3 Blade element kinematics

Velocity

The linear and angular velocity in the fixed hub reference frame are transformed to the rotating hub reference frame. The two frames share the same origin; the rotation angle between the nonrotating and rotating hub coordinate systems is given by the reference blade azimuth position ψ. Therefore, since the rotor of the simulated helicopter turns counterclockwise (seen from above), it is necessary to correctly evaluate the angular rotation sign (hence the minus in the relation 4.15).

Input linear and angular velocity in fixed hub coordinates are defined by the following vectors:

$$\vec{V}_H = \begin{pmatrix} u_H & v_H & w_H \end{pmatrix}^T \tag{4.13}$$

$$\vec{\omega}_H = \begin{pmatrix} p_H & q_H & r_H \end{pmatrix}^T \tag{4.14}$$

The relative rotational speed between the fixed and the rotating hub coordinates systems is defined by the following vector:

$$\vec{\omega}_{RH} = \begin{pmatrix} 0 & 0 & -\dot{\psi} \end{pmatrix}^T = \begin{pmatrix} 0 & 0 & -\Omega \end{pmatrix}^T \tag{4.15}$$

Where Ω is the angular velocity of the main rotor.

Velocities in rotating hub frame are evaluated as following:

$$\vec{V}_R = L_{H2R}\vec{V}_H \tag{4.16}$$

$$\omega_R = L_{H2R}\,\vec{\omega}_H + \vec{\omega}_{RH} \tag{4.17}$$

At the end, the linear velocity of the generic blade element is computed:

$$\vec{V}_b = L_{R2b}\vec{V}_{Rb} \tag{4.18}$$

where $\vec{V}_{Rb}$ is the linear velocity of the generic blade element in hub rotating reference frame:

$$\vec{V}_{Rb} = \vec{V}_R + \vec{\omega}_R \times \vec{r}_{Rb} + \dot{\vec{r}}_{Rb} \tag{4.19}$$

and where the $\vec{r}_{Rb}$ is the position vector from the hub center to the generic blade element, as shown in figure 4.3. It is then evaluated as following:

$$\vec{r}_{Rb} = e\vec{c}c + L_{b2R}\,\vec{r} \tag{4.20}$$

with the rotation matrix from the blade reference frame to the rotating hub reference frame defined: $L_{b2R} = L_{R2b}^T$.

The explicit equation of $\vec{V}_b$ is computed:

$$\vec{V}_b = \begin{pmatrix} r\left[\cos(\beta)\,\left(\Omega - r_H + \dot{\zeta}\right) + p_H\cos(\psi+\zeta)\,\sin(\beta) - q_H\sin(\psi+\zeta)\,\sin(\beta)\right] + \\ +v_H\cos(\psi+\zeta) + u_H\sin(\psi+\zeta) + ecc\cos(\zeta)\,(\Omega - r_H) \\ \\ ecc\left[\cos(\beta)\,(\Omega\sin(\zeta) - r_H\sin(\zeta)) - \sin(\beta)\,(q_H\cos(\psi) + p_H\sin(\psi))\right] + \\ -w_H\sin(\beta) - u_H\cos(\psi+\zeta)\,\cos(\beta) + v_H\sin(\psi+\zeta)\,\cos(\beta) \\ \\ ecc\left[\sin(\beta)\,(\Omega\sin(\zeta) - r_H\sin(\zeta)) + \cos(\beta)\,(q_H\cos(\psi) + p_H\sin(\psi))\right] + \\ +w_H\cos(\beta) + r\left[q_H\cos(\psi+\zeta) - \dot{\beta} + p_H\sin(\psi+\zeta)\right] + \\ -u_H\cos(\psi+\zeta)\,\sin(\beta) + v_H\sin(\psi+\zeta)\,\sin(\beta) \end{pmatrix} \tag{4.21}$$

$\vec{V}_b$ represents the velocity components in blade reference frame of the blade element. It is located at r distance from the hinge of the b^{th} blade, which is measured at ψ azimuth from the zero reference azimuth that is pointing at the aft of the helicopter.

It is important to remember that no therms are neglected yet.

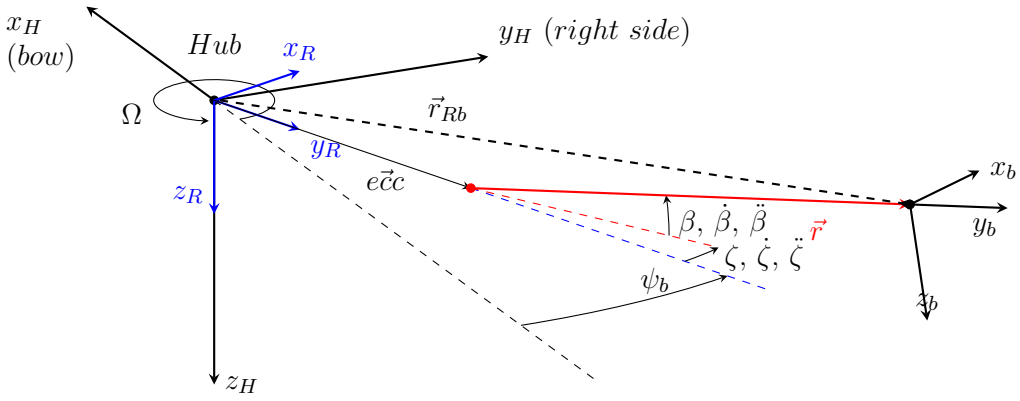

Figure 4.3. Representation of $\vec{r}_{Rb}$

Accelerations

Accelerations of the generic blade element are necessary to evaluate the inertial load to compute the momentum equilibrium at the hinge and to evaluate in the end the $\ddot{\beta}$ and $\ddot{\zeta}$.

Two accelerations are useful in the calculations, respectively the blade element acceleration in blade frame, to evaluate the blade dynamic equation, and the individual acceleration in blade non rotating hub frame, to evaluate the inertial loads transmitted to the shaft. The latter is evaluated as following:

$$\vec{a}_{H\,(b)} \;=\; \dot{\vec{V}}_{H\,(b)} \;+\; \vec{\omega}_H \times \vec{V}_{H\,(b)} \tag{4.22}$$

where $\vec{V}_{H\,(b)}$ is the blade linear velocity evaluated in the fixed hub frame and $\vec{V}_{R\,(b)}$ is the blade element velocity evaluated at equation 4.19:

$$\vec{V}_{H\,(b)} \;=\; L_{R2H}\,\vec{V}_R \tag{4.23}$$

Blade element linear acceleration in blade reference frame is evaluated by transforming the $\vec{a}_{H\,(b)}$ as following:

$$\vec{a}_b \;=\; L_{R2b}\,L_{H2R}\,\vec{a}_{H\,(b)} \tag{4.24}$$

The resulting explicit formulations are now reported. Since the $a_{b\,y\,(b)}$ component is not used in the model, this is not computed.

$$\begin{aligned}
a_{H\,x\,(b)} \;&= \dot{u}_h + q_h\,w_h - r_h\,v_h + \\
&+ r\Big\{\cos(\beta)\Big[\cos(\psi+\zeta)\,\Big(\dot{\beta}^2 + \Omega^2 - 2\,\Omega\,r_h + 2\,\Omega\,\dot{\zeta} + {q_h}^2 + {r_h}^2 + \\
&- 2\,r_h\,\dot{\zeta} + \dot{\zeta}^2\Big) - 2\,\dot{\beta}\,q_h + \sin(\psi+\zeta)\,\Big(\dot{\Omega} - \dot{r}_h + \ddot{\zeta} + p_h\,q_h\Big)\Big] + \\
&- \sin(\beta)\,\Big[\dot{q}_h + \sin(\psi+\zeta)\,\Big(2\,\dot{\beta}\,\Omega + -2\,\dot{\beta}\,r_h + 2\,\dot{\beta}\,\dot{\zeta}\Big) + p_h\,r_h - \ddot{\beta}\cos(\psi+\zeta)\Big]\Big\} + \\
&+ ecc\Big[\sin(\psi)\,\Big(\dot{\Omega} - \dot{r}_h + p_h\,q_h\Big) + \cos(\psi)\,\Big({q_h}^2 + \Omega\,(\Omega - r_h) - r_h\,(\Omega - r_h)\Big)\Big].
\end{aligned} \tag{4.25}$$

$$\begin{aligned}
a_{H\,y\,(b)} \;&= \dot{v}_h - p_h\,w_h + r_h\,u_h + \\
&- ecc\,\Big(\cos(\psi)\,\Big(\dot{r}_h - \dot{\Omega} + p_h\,q_h\Big) + \sin(\psi)\,\Big({p_h}^2 + \Omega\,(\Omega - r_h) - r_h\,(\Omega - r_h)\Big)\Big) + \\
&- r\Big\{\sin(\beta)\,\Big[\cos(\psi+\zeta)\,\Big(2\,\dot{\beta}\,\Omega - 2\,\dot{\beta}\,r_h + 2\,\dot{\beta}\,\dot{\zeta}\Big) - \dot{p}_h + q_h\,r_h + \ddot{\beta}\sin(\psi+\zeta)\Big] + \\
&- \cos(\beta)\,\Big[2\,\dot{\beta}\,p_h - \sin(\psi+\zeta)\,\Big(\dot{\beta}^2 + {p_h}^2 + \Omega^2 - 2\,\Omega\,r_h + 2\,\Omega\,\dot{\zeta} + {r_h}^2 - 2\,r_h\,\dot{\zeta} + \dot{\zeta}^2\Big) + \\
&+ \cos(\psi+\zeta)\,\Big(\dot{\Omega} - \dot{r}_h + \ddot{\zeta} - p_h\,q_h\Big)\Big]\Big\}.
\end{aligned} \tag{4.26}$$

$$
\begin{aligned}
a_{H\,z\,(b)} \; &= \dot{w}_h + p_h\, v_h - q_h\, u_h + \\
&+ ecc\,[\cos(\psi)\;(\dot{q}_h + 2\,p_h\,\Omega - p_h\,r_h) + \sin(\psi)\;(\dot{p}_h - 2\,\Omega\,q_h + q_h\,r_h)] + \\
&+ r\left\{\cos(\beta)\left[\cos(\psi+\zeta)\;\left(\dot{q}_h + 2\,p_h\,\Omega - p_h\,r_h + 2\,p_h\,\dot{\zeta}\right) + \right.\right. \\
&- \ddot{\beta} + \sin(\psi+\zeta)\;\left(\dot{p}_h - 2\,\Omega\,q_h + q_h\,r_h - 2\,q_h\,\dot{\zeta}\right)\Big] + \\
&\left.\left. + \sin(\beta)\;\left[\dot{\beta}^2 - 2\sin(\psi+\zeta)\;\dot{\beta}\,p_h - 2\cos(\psi+\zeta)\;\dot{\beta}\,q_h + {p_h}^2 + {q_h}^2\right]\right\}.
\end{aligned}
\tag{4.27}
$$

$$
\begin{aligned}
a_{b\,x} \; &= ecc\left[\sin(\zeta)\;(\Omega - r_h)^2 - {p_h}^2\,\frac{1}{2}\,(\sin(2\,\psi+\zeta) - \sin(\zeta)) + \right. \\
&\left. + {q_h}^2\,\frac{1}{2}\,(\sin(2\,\psi+\zeta) + \sin(\zeta)) + \cos(\zeta)\;\left(\dot{\Omega} - \dot{r}_h\right) - p_h\,q_h\cos(2\,\psi+\zeta)\right] + \\
&- r\left\{\sin(\beta)\;\left(2\,\dot{\beta}\,\Omega - 2\,\dot{\beta}\,r_h + 2\,\dot{\beta}\,\dot{\zeta}\right) + \right. \\
&- \cos(\beta)\;\left(-\frac{1}{2}\sin(2\,\psi+2\,\zeta)\;{p_h}^2 - \cos(2\,\psi+2\,\zeta)\;p_h\,q_h + \frac{1}{2}\sin(2\,\psi+2\,\zeta)\;{q_h}^2 + \dot{\Omega} - \dot{r}_h + \ddot{\zeta}\right) + \\
&- \cos(\psi+\zeta)\;\left(\sin(\beta)\;(\dot{p}_h - q_h\,r_h) + 2\,\dot{\beta}\,p_h\cos(\beta)\right) + \\
&\left. + \sin(\psi+\zeta)\;\left(\sin(\beta)\;(\dot{q}_h + p_h\,r_h) + 2\,\dot{\beta}\,q_h\cos(\beta)\right)\right\} + \\
&+ \cos(\psi+\zeta)\;(\dot{v}_h - p_h\,w_h + r_h\,u_h) + \sin(\psi+\zeta)\;(\dot{u}_h + q_h\,w_h - r_h\,v_h).
\end{aligned}
\tag{4.28}
$$

$$
\begin{aligned}
a_{b\,z} \; = & \cos(\beta)\;(\dot{w}_h + p_h\,v_h - q_h\,u_h) - r\Big\{\ddot{\beta}\cos(\beta)^2 + \\
& - \sin(\psi+\zeta)\;\Big[\Big(\dot{p}_h - 2\,\Omega\,q_h + q_h\,r_h - 2\,q_h\,\dot{\zeta}\Big)\cos(\beta)^2 + (\dot{p}_h - q_h\,r_h)\sin(\beta)^2\Big] + \\
& - \cos(\psi+\zeta)\;\Big[\Big(\dot{q}_h + 2\,p_h\,\Omega - p_h\,r_h + 2\,p_h\,\dot{\zeta}\Big)\cos(\beta)^2 + (\dot{q}_h + p_h\,r_h)\sin(\beta)^2\Big] + \\
& + \ddot{\beta}\sin(\beta)^2 + \cos(\beta)\;\sin(\beta)\;\Big[\frac{1}{2}\left(-\cos(2\,\psi+2\,\zeta)-1\right){p_h}^2 + \\
& + \sin(2\,\psi+2\,\zeta)\;p_h\,q_h + \Omega^2 - 2\,\Omega\,r_h + 2\,\Omega\,\dot{\zeta} + \frac{1}{2}\left(\cos(2\,\psi+2\,\zeta)-1\right){q_h}^2 + \\
& + {r_h}^2 - 2\,r_h\,\dot{\zeta} + \dot{\zeta}^2\Big]\Big\} + \\
& + ecc\cos(\beta)\;[\cos(\psi)\;(\dot{q}_h + 2\,p_h\,\Omega - p_h\,r_h) + \sin(\psi)\;(\dot{p}_h - 2\,\Omega\,q_h + q_h\,r_h)] + \\
& - \cos(\psi+\zeta)\;\sin(\beta)\;(\dot{u}_h + q_h\,w_h - r_h\,v_h) + \\
& + \sin(\psi+\zeta)\;\sin(\beta)\;(\dot{v}_h - p_h\,w_h + r_h\,u_h) + \\
& - ecc\sin(\beta)\;\Big[{q_h}^2\,\frac{1}{2}\left(\cos(2\,\psi+\zeta)+\cos(\zeta)\right) - {p_h}^2\,\frac{1}{2}\left(\cos(2\,\psi+\zeta)-\cos(\zeta)\right) + \\
& + \cos(\zeta)\;(\Omega - r_h)^2 - \sin(\zeta)\;\Big(\dot{\Omega} - \dot{r}_h\Big) + p_h\,q_h\sin(2\,\psi+\zeta)\Big]
\end{aligned}
\tag{4.29}
$$

4.1.4 Aerodynamic loads

Rotor blade aerodynamics modeling is based on the blade element theory. The blade is spatially discretized along the blade span. The forces and moments acting on each individual blade element are evaluated and the total loads acting on the entire blade are obtained by integrating these forces on the discretization.

In this modeling, the properties of the blade element, such as the chord, the geometric twist, the airfoil, etc. are assigned to a point lying along the opening of the same.

The aerodynamic analysis carried out on the blade element are obviously not in real time but are obtained through interpolation of tabulated data.

The data used in this model are only the C_L and C_D, in fact the contribution of the aerodynamic pitching moment (C_m)is neglected, as there is no pitching dynamic in the model except the one of the pitch control.

The aerodynamic computation to obtain these data were carried out with the CFD on 20 different bi-dimensional sections of the blade (therefore 20 airfoils), on a stationary and compressible domain. The aerodynamics of the blade in this model can therefore be considered:

- 2D
- with stationary coefficients

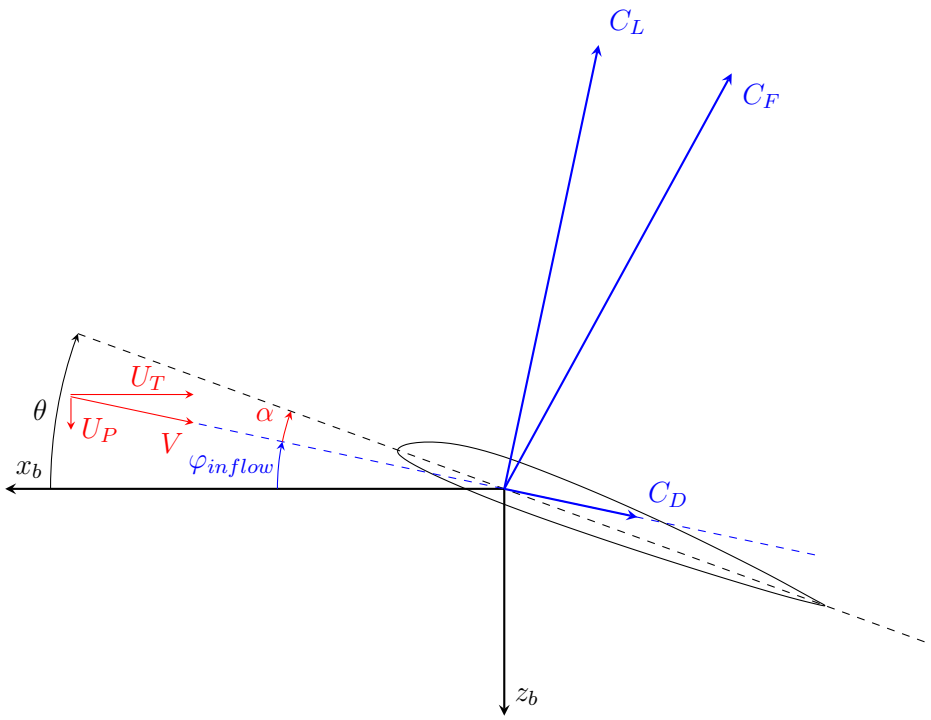

Figure 4.4. Blade angles and velocity in blade-element reference frame

- compressible (up to high subsonic or transonic, where, however any hypotheses about steadiness and bi-dimensional flow decays).

The 2D polar are defined over a range of 360° angle of attack through interpolation-reconstruction methods. This wide range of angle of attack allows to evaluate the reverse flow and the local blade stall (but not the dynamic stall).

For the evaluation of the aerodynamic loads it is therefore necessary to determine the local incident speeds on the airfoil of the generic element. Subsequently, it is possible to calculate the angle of attack, the total velocity and the Mach of the flow. Finally, it is possible to interpolate from the tables.

The local speed of the blade element in the respective reference system is calculated by transforming the linear and angular speeds of the helicopter in these coordinates. The result of the transformation is reported in the set of equations 4.18. However, these speeds are not the ones that really represent the flow field at the airfoil location (i.e. blade element): in fact, the contribution of the speeds induced to the rotor disc is missing. From the inflow model discussed thoroughly in chapter 4.1.9, it is possible to obtain a triangle of induced speeds to correct those deriving from the kinematics of the helicopter and the rotor.

Usually in literature those speeds of the blade element are defined by three components, tangential, perpendicular and radial, as shown in Figure 4.4, specifically with the radial

component entering the x_b - z_b plane. However, this definition is consistent with the proposed reference system, called blade element referent frame.

$$\vec{U}_b = \begin{pmatrix} U_t & U_r & U_p \end{pmatrix}^T \tag{4.30}$$

The resulting velocity components are evaluated according to the following correction:

$$\vec{U}_b = \vec{V}_b + \vec{V}_{inflow} \tag{4.31}$$

with $\vec{V}_{inflow}$ as the inflow velocity vector in the blade reference frame, as explained in chapter 4.1.9. With this approach it is possible to easily change the inflow model .

The resulting local velocity $\vec{U}_b$ is used to compute the angle of attack and the Mach of the flow to interpolate the aerodynamic coefficients of the blade element. To estimate the angle of attack α of the generic blade station located at a radial distance r from the flap-lead hinge a budget of contributions is computed:

$$\alpha = \theta_G + \varphi \tag{4.32}$$

where φ is the angle of the flow at the blade element and θ_G is the geometric pitch composed by the control contribution.

The local geometrical construction twist is then calculated as following:

$$\theta_G = \theta_0 + A_{1s}\cos(\psi) + B_{1c}\sin(\psi) + \theta_{twist} \tag{4.33}$$

where θ_0 is the constant collective pitch angle and A_{1s} and B_{1c} are the control contribution from the cyclic control. Since ψ is measured from the rearmost position of the blade, a positive value of B_{1c} gives a forward (nose down) command, while a positive value of A_{1s} gives a sideways command, in the direction of $\psi = 90^o$.

To evaluate the φ, a simple trigonometric projection is computed, as shown in figure 4.4 :

$$\varphi = \tan^{-1}\left(\frac{U_p}{U_t}\right) \tag{4.34}$$

Given the compressible flow hypothesis, the Mach value is also computed:

$$Mach = \frac{V}{c_s} \tag{4.35}$$

where c_s is the local speed of sound and V the flow velocity: $V = \sqrt{U_p^2 + U_t^2}$.

Values of α, $Mach$ and r are now used to interpolate aerodynamic tables of coefficients C_L and C_D.

The aerodynamic force coefficient $\vec{C}_F$ on the k^{th} blade element is evaluated as following, coherently with the reference frame:

$$\vec{C}_{F\,a(i)} = \begin{pmatrix} -C_D\cos(\varphi) - C_L\sin(\varphi) \\ 0 \\ C_D\sin(\varphi) - C_L\cos(\varphi) \end{pmatrix} \tag{4.36}$$

Blade-span Integration

The integration calculation on the discretized blade of the forces of the blade elements is computed numerically. The blade discretization domain is calculated from the flap-lead hinge up to the tip. The implemented discretization is of exponential type and can be configured through a series of parameters:

- Number of elements or nodes. An high number of blades elements leads to a better loads evaluation. However, this value is strongly affecting the code performance in terms of computation time, a very important topic for real-time simulation.
- Stretch factor. It is important to refine the discretization at the blade-tip and-or at the blade root, where large load gradients are present.
- Tip loss and rotor root cutout. The blade integration domain is refined over an effective root and tip. The effective integration domain cuts out the blade portions where the previous flow hypothesis can no longer be considered valid, such as with 3D flow or very disturbed flow by the interactions of wakes or vortex.

The numerical integration is carried out by applying the trapezoidal rule. This numerical integration method has been chosen as it is of simple implementation and performance while still guaranteeing an good approximation of the integral.

For the i^{th} blade element, the force per unit span is evaluated as following:

$$d\vec{F}_{a\,(i)} = \frac{1}{2}\rho V^2 c_b \vec{C}_{F\,a(i)} \tag{4.37}$$

For all the b^{th} blade, the trapezoidal integration method is implemented to evaluate the aerodynamic force in the blade element frame of reference. The total aerodynamic shear force at the hinge, for each blade, is thus evaluated:

$$\vec{F}_{a\,b} = \frac{1}{2}\sum_{i=1}^{N_k} y_{(i)} \left(d\vec{F}_{a\,(i)} + d\vec{F}_{a\,(i+1)} \right) \tag{4.38}$$

where $y_{(i)}$ is the blade element span that is evaluated as: $y_{(i)} = r_{(i+1)} - r_{(i)}$.

Through numerical integration, the aerodynamic moment is also calculated. The aerodynamic moment of the i^{th} blade element per unit span, located at $\vec{r}_i$, is evaluated:

$$d\vec{M}_{a\,(i)} = \vec{r}_i \times d\vec{F}_{a\,(i)} \tag{4.39}$$

The resulting total aerodynamic moment at the hing for each blade is evaluated with trapezoidal integration as following:

$$\vec{M}_{a\,b} = \frac{1}{2}\sum_{i=1}^{N_k} y_{(i)} \left(d\vec{M}_{a\,(i)} + d\vec{M}_{a\,(i+1)} \right) = \begin{pmatrix} M_{a\,\beta} & 0 & M_{a\,\zeta} \end{pmatrix}^T \tag{4.40}$$

Total aerodynamic loads

Aerodynamic load transmitted to the shaft, and therefore to the helicopter, are only those from shear forces on the flap-lead hinge. Those loads are calculated in the blade coordinate system. Hence, they must be transported in the fixed Hub frame of reference through the following relations, for each b^{th} blade.

Shear force in fixed hub frame is computed with the following transformation:

$$\vec{F}_{a\,H\,(b)} = L_{R2H}\, L_{b2R}\, \vec{F}_{a\,b} \tag{4.41}$$

Shear moment in fixed hub frame is then computed with the following transformation:

$$\vec{M}_{a\,H\,(b)} = L_{R2H} \left(e\vec{c}c \times \left(L_{b2R}\, \vec{F}_{a\,b} \right) \right) \tag{4.42}$$

Those aerodynamic loads will be evaluated for each blade and employed to compose the total output loads sensed by the helicopter.

4.1.5 Blade dynamics governing equation

Articulated blades equations of motion follow the approach proposed in ref. [8]. By enforcing the moment equilibrium around the flap and lead-lag hinges, the equations of motion are formulated, as following:

$$\vec{M}_{a\,b} + \vec{M}_{hs\,b} + \vec{M}_{dmp\,b} + \vec{M}_{w\,b} + \vec{M}_{I\,b} = 0 \tag{4.43}$$

where the $\vec{M}_{hs\,b}$ is the hinge-concentrated-spring moment and $\vec{M}_{dmp\,b}$ is the moment of the damper; both are discussed in Chapter 4.1.6. The aerodynamic moment $\vec{M}_{a\,b}$ is the one previously obtained in equation 4.40. Blade weight moment contribution $\vec{M}_{w\,b}$ could be inserted at this point but in the implemented model is neglected.

Inertial moment contribution $\vec{M}_{I\,b}$ is evaluated by integrating the elementary inertial moment of blade element in blade coordinate system. For a most general discussion, the equations are formulated in a vectorial form:

$$\vec{M}_{I\,b} = \int_r \rho_l \; (\vec{r} \times \vec{a}_b) \; dr \tag{4.44}$$

where $\vec{r}$, as previously shown, is the blade element position vector, which starts at the hinge and points to the i^{th} blade section. A general linear mass density distribution ρ_l is used for the blade, ad is concentrated along the blade span axis (y_b). Accordingly, by analysing the resulting integral computation coefficients, it is possible to isolate the $\left[\frac{1}{2}\,\rho_l\, r^2\right]_r$ therm, that represent the blade moment of inertia I_b, and the $[\rho_l\, r]_r$ therm, that represent the blade static moment of inertia S_b.

Evermore, as a consequence of the hypothesis about the blade mass distribution, the values of the moments of inertia are respectively identical for the flap rotation and the

lead rotation. This substitution permits to use measured values of the inertia moments without computing any mass density distribution. By making explicit the equation 4.43, it is possible to isolate the second order derivatives of the blade dynamic states: $\ddot{\beta}$ and $\ddot{\zeta}$. The complete resulting equations are reported:

$$\begin{aligned}
\ddot{\zeta} \;=\; & -\frac{M_{a\,\zeta} \;+\; M_{hs\,\zeta} + M_{dmp\,\zeta}}{I_b \cos(\beta)} + \\
& + \frac{1}{\cos(\beta)} \Big\{ \sin(\beta)\; \Big(2\,\dot{\beta}\,\Omega - 2\,\dot{\beta}\,r_h + 2\,\dot{\beta}\,\dot{\zeta}\Big) + \\
& - \cos(\psi+\zeta)\; \Big(\sin(\beta)\; (\dot{p}_h - q_h\,r_h) + 2\,\dot{\beta}\,p_h \cos(\beta)\Big) + \\
& + \sin(\psi+\zeta)\; \Big(\sin(\beta)\; (\dot{q}_h + p_h\,r_h) + 2\,\dot{\beta}\,q_h \cos(\beta)\Big) + \\
& + \cos(\beta)\; \Big(\frac{1}{2}\sin(2\,\psi+2\,\zeta)\; {p_h}^2 + \cos(2\,\psi+2\,\zeta)\; p_h\,q_h - \frac{1}{2}\sin(2\,\psi+2\,\zeta)\; {q_h}^2 - \dot{\Omega} + \dot{r}_h\Big)\Big\} + \\
& - \frac{S_b}{I_b \cos(\beta)} \Big\{ ecc \Big[\sin(\zeta)\; (\Omega - r_h)^2 - {p_h}^2 \Big(\frac{1}{2}\sin(2\,\psi+\zeta) + -\frac{1}{2}\sin(\zeta)\Big) + \\
& + {q_h}^2 \Big(\frac{1}{2}\sin(2\,\psi+\zeta) + \frac{1}{2}\sin(\zeta)\Big) + \cos(\zeta)\; \Big(\dot{\Omega} - \dot{r}_h\Big) - p_h\,q_h \cos(2\,\psi+\zeta)\Big] + \\
& + \cos(\psi+\zeta)\; (\dot{v}_h - p_h\,w_h + r_h\,u_h) + \sin(\psi+\zeta)\; (\dot{u}_h + q_h\,w_h - r_h\,v_h)\Big\}.
\end{aligned} \tag{4.45}$$

$$\begin{aligned}
\ddot{\beta} \;=\; & -\frac{M_{a\,\beta} \;+\; M_{hs\,\beta} + M_{dmp\,\beta}}{I_b} + \\
& \cos(\psi+\zeta)\; \Big(\Big(\dot{q}_h + 2\,p_h\,\Omega - p_h\,r_h + 2\,p_h\,\dot{\zeta}\Big)\cos(\beta)^2 + (\dot{q}_h + p_h\,r_h)\sin(\beta)^2\Big) + \\
& + \sin(\psi+\zeta)\; \Big(\Big(\dot{p}_h - 2\,\Omega\,q_h + q_h\,r_h - 2\,q_h\,\dot{\zeta}\Big)\cos(\beta)^2 + (\dot{p}_h - q_h\,r_h)\sin(\beta)^2\Big) + \\
& - \cos(\beta)\; \sin(\beta) \Big\{ \frac{1}{2}\,(-\cos(2\,\psi+2\,\zeta) - 1)\,{p_h}^2 + \sin(2\,\psi+2\,\zeta)\; p_h\,q_h + \\
& + \Omega^2 - 2\,\Omega\,r_h + 2\,\Omega\,\dot{\zeta} + \frac{1}{2}\,(\cos(2\,\psi+2\,\zeta) - 1)\,{q_h}^2 + {r_h}^2 - 2\,r_h\,\dot{\zeta} + \dot{\zeta}^2\Big\} + \\
& + \frac{S_b}{I_b} \Big\{ \cos(\beta)\; (\dot{w}_h + p_h\,v_h - q_h\,u_h) + ecc\cos(\beta)\; \big(\cos(\psi)\; (\dot{q}_h + 2\,p_h\,\Omega - p_h\,r_h) + \\
& + \sin(\psi)\; (\dot{p}_h - 2\,\Omega\,q_h + q_h\,r_h)\big) - \cos(\psi+\zeta)\; \sin(\beta)\; (\dot{u}_h + q_h\,w_h - r_h\,v_h) + \\
& + \sin(\psi+\zeta)\; \sin(\beta)\; (\dot{v}_h - p_h\,w_h + r_h\,u_h) + \\
& - ecc\,\sin(\beta)\; \Big[{q_h}^2\,\frac{1}{2}\,(\cos(2\,\psi+\zeta) + \cos(\zeta)) - {p_h}^2\,\frac{1}{2}\,(\cos(2\,\psi+\zeta) - \cos(\zeta)) + \\
& + \cos(\zeta)\; (\Omega - r_h)^2 - \sin(\zeta)\; \Big(\dot{\Omega} - \dot{r}_h\Big) + p_h\,q_h \sin(2\,\psi+\zeta)\Big]\Big\}.
\end{aligned} \tag{4.46}$$

It is important to underline that no therms are neglected in the equations 4.46, 4.45. This, as it can be seen, generates a quite complicated set of equations. In fact, a great effort has been put into managing the simplification of the equations with the Matlab® symbolic script in order to obtain equations that can still be interpreted and implemented easily. The Matlab® has been translated into C++ code language, the language in which the simulator is developed.

4.1.6 Hinge-Spring and Lag Damper models

As explained in the model hypothesis, the lead-lag and flap blade rotation occur about a hinge located at a distance from the hub with the eccentricity *ecc*. To simulate the hingeless helicopter main rotor the "live hinge" (or elastic hinge) stiffness is simulated by a pair of hinge-concentrated springs, one for the flap and one for the lead-lag degrees of freedom. The representation of stiffness by means of concentrated spring is an approach frequently used for hingeless rotors [1] [12]. Physical values of equivalent hinge stiffness are estimated from the Lynx and the BO-105 data collected by Padfield [12].

In the same way, a hinge-concentrated damper is added to the model for both flap and lead-lag blades degrees of freedom. The lag damper is extensively used in helicopter rotors, both hinged and hingeless ones. However, the lag dampers kinematic varies a lot for each helicopter and, in to maintain a certain level of generality, it is modelled as hinge-concentrated, with a linear response to angular velocity.

On the other hand, flap dampers are rarely or never mounted on helicopters: they are exploited in this model to enhance the configurability with hypothetical physical parameter to fine-tune the model; however, by default, the value of flap damping is set to zero.

The loads of those elements are evaluated in the blade reference frame and are moments about the hinge, evaluated as following:

$$\vec{M}_{hs\,b} = \begin{pmatrix} -k_\beta\,\beta_b \\ 0 \\ k_\zeta\,\zeta_b \end{pmatrix} \tag{4.47}$$

$$\vec{M}_{dmp\,b} = \begin{pmatrix} -c_\beta\,\dot{\beta}_b \\ 0 \\ c_\zeta\,\dot{\zeta}_b \end{pmatrix} \tag{4.48}$$

where k_β and k_ζ are the springs stiffness expressed in $[N/rad]$, and c_β and c_ζ are the damping of the dampers expressed in $[N/rad^2]$.

As additional configuration to the model, it is possible to switch-off the lead-lag dof.

To easily resolve the degradation of the model, it is mandatory to make changes to simulate an infinite-rigid lead-lag hinge (i.e. lead-lag hinge nonexistence). In addition to keeping the values of the lag states (and derivatives) null, it is necessary to correctly evaluate the moments that compose the shaft torque. Therefore, the aerodynamic moment

$M_{a\zeta}$ about the z axis, evaluated by equation 4.40, must be transmitted to the shaft by modifying the equation 4.47 as following:

$$\vec{M}_{hs\,b} = \begin{pmatrix} -k_\beta\,\beta_b \\ 0 \\ M_{a\,\zeta} \end{pmatrix} \tag{4.49}$$

The artifice to switch-off the 3 dof of lead-lag blade dynamic was a fundamental step in the development and implementation of the model. The model was implemented using the equations relevant to 6 dofs but the first tests, which were about debugging, cleaning, and evaluation of the implemented equations, were carried out keeping the lag dynamics off. The modular approach, used also in the development of the model, was fundamental both to verify the robustness of the code and to evaluate the improvements brought from a higher level modeling.

The moments exchanged by the dampers and the springs at the hinges are also transmitted through the shaft to the helicopter body, thus they compete with the overall loads budget. The transformation to the fixed Hub reference frame is expressed as usual:

$$\vec{M}_{hs\,H\,(b)} = L_{R2H}\,L_{b2R}\,\vec{M}_{hs\,b} \tag{4.50}$$

$$\vec{M}_{dmp\,H\,(b)} = L_{R2H}\,L_{b2R}\,\vec{M}_{dmp\,b} \tag{4.51}$$

4.1.7 Shaft-transmitted inertial loads

The inertial loads that are transmitted by the shaft to the fuselage are evaluated by integrating the blade accelerations in the non-rotating hub frame, previously evaluated in equation 4.22. Those loads are shear forces transmitted to the shaft through the hinges and are evaluated as following:

$$\vec{F}_{I\,H\,(b)} = \int_r \rho_l\,\vec{a}_{H\,(b)}\,dr \tag{4.52}$$

By solving the integral, it is possible to replace the therm $[\rho_l\,r]_r$ with the blade static moment of inertia I_S, and the therm $[\rho_l]_r$ with the blade mass m_b. Thus, as done for the blade dynamic equations, the substitution permits a more general level of model implementation.
Explicit equations for each blade are finally computed:

$$
\begin{aligned}
F_{I\,H\,x\,(b)} \;=\; & -S_b \Big\{ \cos(\beta) \Big[\cos(\psi+\zeta) \left(\dot{\beta}^2 + \Omega^2 - 2\,\Omega\,r_h + 2\,\Omega\,\dot{\zeta} + {q_h}^2 + {r_h}^2 - 2\,r_h\,\dot{\zeta} + \dot{\zeta}^2 \right) + \\
& - 2\,\dot{\beta}\,q_h + \sin(\psi+\zeta) \left(\dot{\Omega} - \dot{r}_h + \ddot{\zeta} + p_h\,q_h \right) \Big] + \\
& - \sin(\beta) \left[\dot{q}_h + \sin(\psi+\zeta) \left(2\,\dot{\beta}\,\Omega - 2\,\dot{\beta}\,r_h + 2\,\dot{\beta}\,\dot{\zeta} \right) + p_h\,r_h - \ddot{\beta}\cos(\psi+\zeta) \right] \Big\} + \\
& - m_b \Big\{ \dot{u}_h + q_h\,w_h - r_h\,v_h + ecc \Big[\sin(\psi) \left(\dot{\Omega} - \dot{r}_h + p_h\,q_h \right) + \\
& + \cos(\psi) \left({q_h}^2 + \Omega\,(\Omega - r_h) - r_h\,(\Omega - r_h) \right) \Big] \Big\}
\end{aligned}
\tag{4.53}
$$

$$
\begin{aligned}
F_{I\,H\,y\,(b)} \;=\; & S_b \Big\{ \sin(\beta) \left(\cos(\psi+\zeta) \left[2\,\dot{\beta}\,\Omega - 2\,\dot{\beta}\,r_h + 2\,\dot{\beta}\,\dot{\zeta} \right] - \dot{p}_h + q_h\,r_h + \ddot{\beta}\sin(\psi+\zeta) \right) + \\
& - \cos(\beta) \Big[2\,\dot{\beta}\,p_h - \sin(\psi+\zeta) \left(\dot{\beta}^2 + {p_h}^2 + \Omega^2 - 2\,\Omega\,r_h + 2\,\Omega\,\dot{\zeta} + {r_h}^2 - 2\,r_h\,\dot{\zeta} + \dot{\zeta}^2 \right) + \\
& + \cos(\psi+\zeta) \left(\dot{\Omega} - \dot{r}_h + \ddot{\zeta} - p_h\,q_h \right) \Big] \Big\} + \\
& - m_b \Big\{ \dot{v}_h - p_h\,w_h + r_h\,u_h - ecc \Big[\cos(\psi) \left(\dot{r}_h - \dot{\Omega} + p_h\,q_h \right) + \\
& + \sin(\psi) \left({p_h}^2 + \Omega\,(\Omega - r_h) - r_h\,(\Omega - r_h) \right) \Big] \Big\}
\end{aligned}
\tag{4.54}
$$

$$
\begin{aligned}
F_{I\,H\,z\,(b)} \;=\; & -m_b \Big\{ \dot{w}_h + ecc \Big[\cos(\psi) \left(\dot{q}_h + 2\,p_h\,\Omega - p_h\,r_h \right) + \sin(\psi) \left(\dot{p}_h - 2\,\Omega\,q_h + q_h\,r_h \right) \Big] + \\
& + p_h\,v_h - q_h\,u_h \Big\} + \\
& - S_b \Big\{ \cos(\beta) \Big[\cos(\psi+\zeta) \left(\dot{q}_h + 2\,p_h\,\Omega - p_h\,r_h + 2\,p_h\,\dot{\zeta} \right) - \ddot{\beta} + \\
& + \sin(\psi+\zeta) \left(\dot{p}_h - 2\,\Omega\,q_h + q_h\,r_h - 2\,q_h\,\dot{\zeta} \right) \Big] + \\
& + \sin(\beta) \left[\dot{\beta}^2 - 2\sin(\psi+\zeta)\,\dot{\beta}\,p_h - 2\cos(\psi+\zeta)\,\dot{\beta}\,q_h + {p_h}^2 + {q_h}^2 \right] \Big\}
\end{aligned}
\tag{4.55}
$$

The moments generated by the inertial forces in hub reference frame are evaluated as following:

$$
\vec{M}_{I\,H\,(b)} \;=\; \vec{r}_{ecc\,H} \times \vec{F}_{I\,H\,(b)} \tag{4.56}
$$

where $\vec{r}_{ecc\,H}$ is the hinge vector location in the fixed hub coordinates defined as following:

$$\vec{r}_{ecc\,H} = L_{R2H}\, e\vec{c}c = \begin{pmatrix} -ecc\cos(\psi) \\ ecc\sin(\psi) \\ 0 \end{pmatrix} \tag{4.57}$$

The sum of each blade inertial forces and moments is also transmitted through the shaft to the helicopter body, thus they compete with the overall loads budget: that will be computed in chapter 4.1.8.

4.1.8 Total main rotor loads to the Helicopter

In conclusion, the sum of the loads generated by the main rotor that are transmitted to the hub are computed and transformed to the body frame of reference:

$$\vec{F}_H = \sum_{b=1}^{N} \vec{F}_{a\,H\,(b)} + \vec{F}_{I\,H\,(b)} \tag{4.58}$$

Aerodynamic shear forces through the hinges and inertial forces are the only aerodynamic loads to be directly transmitted to the hub. The total moment with the springs and damper contributions is evaluated by the following sum:

$$\vec{M}_H = \sum_{b=1}^{N} \vec{M}_{a\,H\,(b)} + \vec{M}_{I\,H\,(b)} \vec{M}_{dmp\,H\,(b)} + \vec{M}_{hs\,H\,(b)} \tag{4.59}$$

Finally, the loads evaluated in the fixed hub frame of reference can be transferred to the body reference system as following:

$$\vec{F}_B = L_{H2B}\, \vec{F}_H \tag{4.60}$$

$$\vec{M}_B = L_{H2B}\, \vec{M}_H + \vec{r}_{BH} \times \vec{F}_B \tag{4.61}$$

Where the transformation matrix L_{H2B} is evaluated by computing the inverse matrix of 4.1.

The rotor torque Q is evaluated from the third element of the hub frame moment vector $Q = \vec{M}_{H,z}$.

4.1.9 Inflow model

The inflow model implemented in this second part of this work is the one already used in the original model. By maintaining the same inflow sub-model, it is possible to evaluate in the first step the actual improvements made with the new model presented so far.

The model implemented is the one described by Pitt and Peters in ref. [13]. This sub-model has been considered in line with the desired level of the new rotor model.

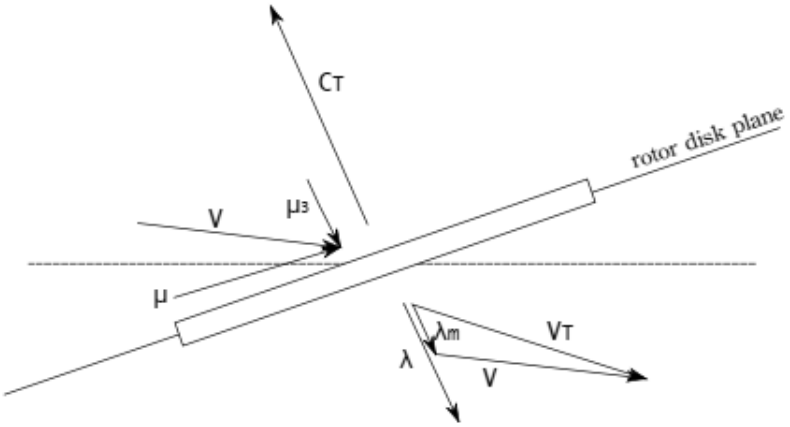

Figure 4.5. Inflow reference diagram, wind axis

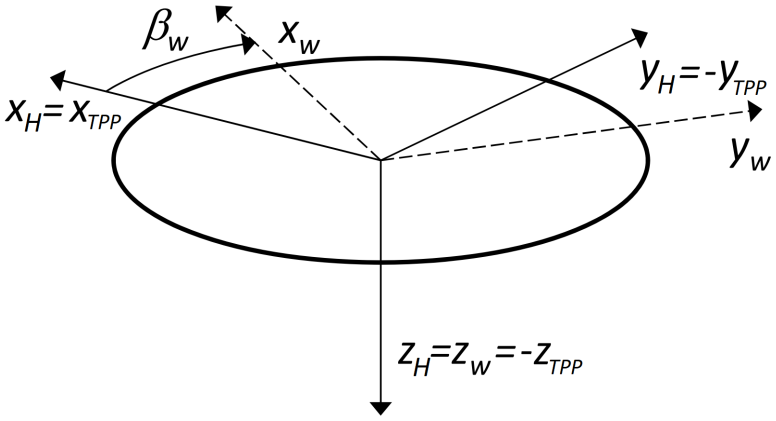

Figure 4.6. Fixed hub, tip path plane and hub-wind axis

Furthermore, the increased complexity of implementing a new model was considered not necessary at this stage of the development. However, this sub-model is also referred in literature as one of the most used for real time simulation rotor models.

The Pitt-Peters model is of the non-stationary type, with three degrees of freedom, and it treats the inflow variables as states of the dynamic.

The velocity flow field is modeled through a triangular velocity distribution, written in hub-wind axis. The three states are named λ_0, λ_{1c} and λ_{1s}, and are respectively the uniform, lateral, and longitudinal variations in rotor inflow.

The velocity field is therefore described as following:

$$v\,(x,\psi) = \Omega\,R\,\left(\lambda_0 + x\,\lambda_s \sin\,(\psi) + x\,\lambda_c \cos\,(\psi)\right) \tag{4.62}$$

where $x = (ecc + r)/R$ is the non-dimensional position along blade span.

The induced flow distributions are assumed to be linear functions of three generalized loads on the rotor.

These loading factors are expressed as non dimensional coefficients, computed as following:

$$C_{loads\,TPP} = \begin{bmatrix} C_T = \frac{T}{\rho\pi R^2(\Omega R)^2} \\ C_l = \frac{L_a}{\rho\pi R^3(\Omega R)^2} \\ C_m = \frac{M_a}{\rho\pi R^3(\Omega R)^2} \end{bmatrix} \tag{4.63}$$

The load coefficients are representing respectively the thrust, roll and pitch moment. In equations 4.63 the longitudinal and lateral terms are expressed in the tip-path-plane coordinate system and must be transformed into the hub-wind reference frame in which it is developed the inflow model. The two coordinates systems are rotated by an angle β_w that is evaluated from the u_H and v_H components of the fixed hub frame velocity, as following:

$$\beta_w \;=\; \sin^{-1}\left(v_h^2\,/\sqrt{u_h^2 + v_h^2}\right) \tag{4.64}$$

The rotation matrix to apply to the load coefficients to transform them from the tip path plane reference frame to the hub-wind reference frame is computed by applying the rotation sequence: $\begin{pmatrix} 0 & 0 & \beta_w \end{pmatrix}$, as shown in figure 4.1.9. The resulting transformation matrix is expressed as following:

$$L_{TPP2w} = \begin{bmatrix} \cos\,(\beta_w) & \sin\,(\beta_w) & 0 \\ -\sin\,(\beta_w) & \cos\,(\beta_w) & 0 \\ 0 & 0 & 1 \end{bmatrix} \tag{4.65}$$

Therefore, the transformation of the coefficients is performed as following:

$$C_{loads\,wind} \;=\; L_{TPP2w}\,C_{loads\,TPP}. \tag{4.66}$$

The load coefficients are evaluated and transformed to the tip path plane from the fixed hub frame as following:

$$T = -F_{a\,H\,,i} \tag{4.67}$$

where $F_{a\,H\,,i}$ is the first component of the total aerodynamic force in hub reference frame, thus the thrust.

$$L = -M_{disk\,H\,,j} \tag{4.68}$$

$$M = M_{disk\,H\,,k} \tag{4.69}$$

where $\vec{M}_{disk\,H}$ is the moment vector used for the inflow model and it is evaluated as following:

$$\vec{M}_{disk\,H} = (M_{disk\,H\,,i}, M_{disk\,H\,,j}, M_{disk\,H\,,k}) = L_{R2H}\, L_{b2R} \left(\vec{M}_{a\,b} + \vec{M}_{hs} + \vec{M}_{dmp}\right) \tag{4.70}$$

Since the inflow model was already developed and implemented, it will not be explored further and a detailed explanation of the model can be found in ref. [13] and [6].

Therefore, it is important to say that the three loads input will be transformed from the Tip Path Plane coordinate system to hub-wind coordinate system.

The contribution of the inflow to the local velocity components used in the equation 4.30 and resulting from the application of this model are:

$$\vec{U}_{inflow} = \begin{pmatrix} 0 \\ -R\,\Omega \sin(\beta) \left(\lambda_0 + \frac{r\,(\lambda_c \cos(\psi+\zeta)+\lambda_s \sin(\psi+\zeta))+\mathrm{ecc}\,(\lambda_c \cos(\psi)+\lambda_s \sin(\psi))}{R}\right) \\ -R\,\Omega \cos(\beta) \left(\lambda_0 + \frac{r\,[\lambda_c \cos(\psi+\zeta)+\lambda_s \sin(\psi+\zeta)]+\mathrm{ecc}\,[\lambda_c \cos(\psi)+\lambda_s \sin(\psi)]}{R}\right) \end{pmatrix} \tag{4.71}$$

The resulting velocity vector is already transformed in the blade element frame of reference.

The output of the inflow sub-model are the inflow state derivatives: $\dot{\lambda}_0$, $\dot{\lambda}_c$ and $\dot{\lambda}_s$. They are treated as states derivatives of the rotor dynamic and therefore, used in the time integration of the flight dynamic model.

4.2 Code implementation scheme

The code implementation work was undoubtedly the most challenging part of the thesis work.
During the initial steps of code design and model implementation, great importance has always been given to modularity, generality and performance of the code.

A modular architecture allows to modify and evolve the model in a simple way, guaranteeing the desired level of generality. Future evolution of the main rotor model can be carried out more easily with the new developed code. Particular attention was also given to the calculation processes and data flow within the code, in order to minimize the computational load requirement.

The computational load in real time simulator is measured with computation time. The real time simulation takes place with a frequency from 60Hz to 120Hz, allowing $16ms$ to $8ms$ for the whole step simulation process. The maximum time allowed for the flight model module (e.g. main rotor, tail rotor, fuselage, horizontal tail, etc.) is less than the half time step.

Table 4.1 shows a summary scheme of the implementation of the code and of the data flow.

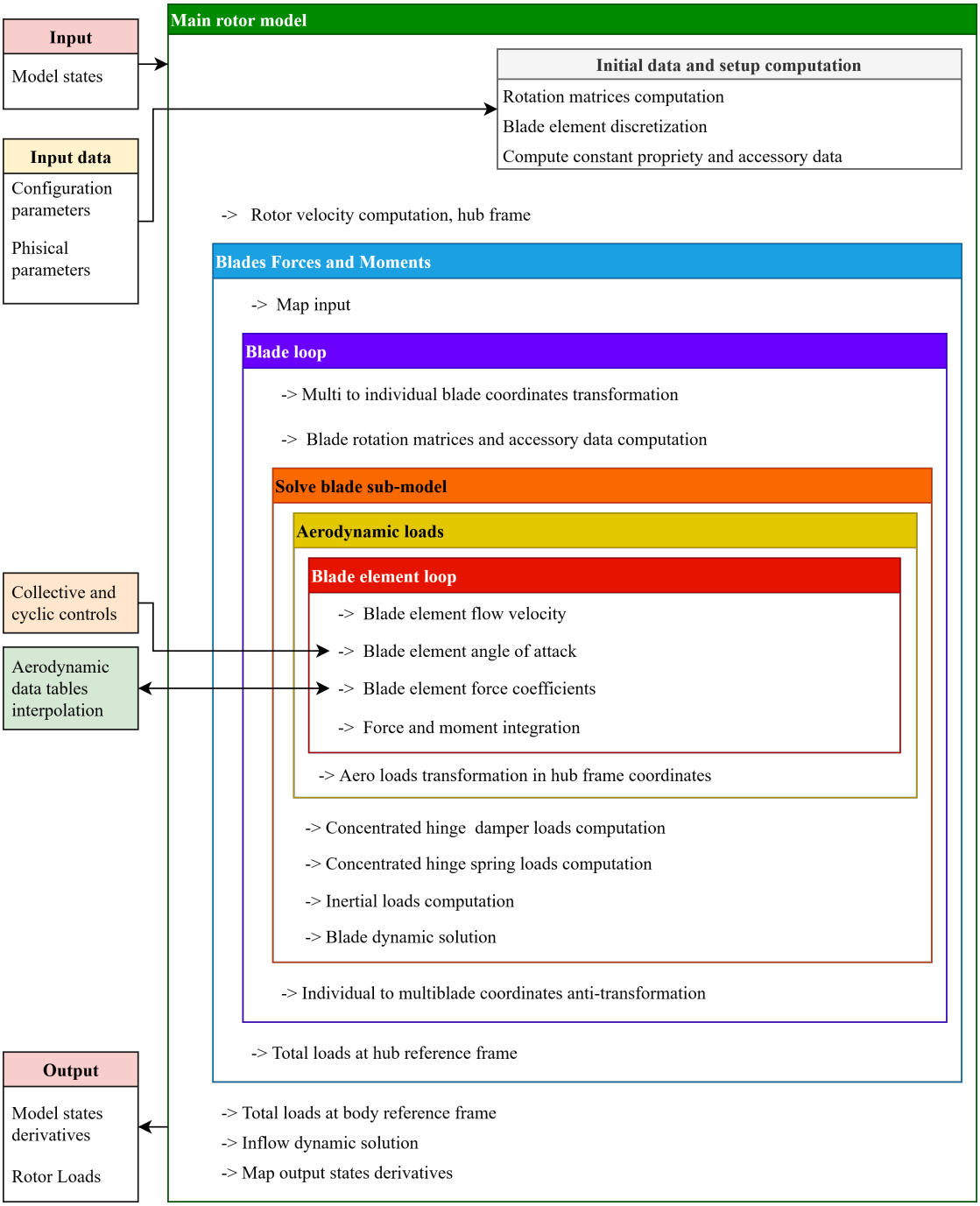

Table 4.1. Model implementation scheme

Chapter 5

Results

This chapter shows the results obtained with the new main rotor model, making a comparison with both the data from the model developed in first part of this work and from the flight tests.
It must be highlighted that the purpose of the second part of this work is to develop a more rigorous model and to obtain a correct off-axis response.

The validation of this new model, at this point of development, is therefore to be considered of a qualitative type. In fact, we want to evaluate the physical quality of the model without any type of tuning activated. The tests are in fact carried out without the use of any level of tuning but only with the use of the characteristic physical parameters of blades and rotor. Furthermore, the values used for these physical parameters are as faithful as possible to those of the simulated helicopter, partly measured, partly obtained from manuals and partly estimated through literature data and comparisons with similar aircraft or configurations.

The results are therefore observed in a qualitative manner rather than analyzing them in compliance with the tolerances. In fact, the model tuning task is not part of this work and will be carried out in the future.

The simulated flight tests are compared with the real flight data and with the model obtained in the first part of the work through overplots. It is important to underline that the old model has already tuning correction in both performance and dynamics, while the new one, as mentioned, does not. Despite this, the new model turns out to work better.

It seemed appropriate to carry out the validation of the model, even if qualitative, through tests that respected as much as possible the behavior of the rotor without having any contributions from other elements of the helicopter. To do this, particular importance was given to hovering tests, as the influence on the flight dynamic of the tail planes and the fuselage can be neglected. In fact, in advanced flight, the tail planes and the fuselage itself contribute significantly to the dynamic due to the aerodynamic loads they develop.

The tests observed during the development and the implementation phase were numerous, both static and dynamic. In this work, however, only two cases of dynamic command response tests are shown, because they were considered sufficiently representative of the

results obtained. All the static tests showed excellent results also comparing with those of the old model. The two dynamic tests proposed are also based on standard tests, one representing the dynamic response to a longitudinal cyclic command (forward input) and the other representing the dynamic response to a lateral cyclic command (left input); these are respectively named by the regulation 2.b.3 (i) and 2.b.3 (ii). It is important to remember that the tests are carried out with the autopilot off, in both the real and the simulated helicopter tests.

Code Performance

It is possible to observe important results also about the performance of the code. The old flight dynamic model, including the engine model, performed a calculation step using an average time of **2.3 ms**. The integrated states of the rotor model alone, in the old code, are 2 for each blade and 3 for the dynamic inflow, hence a total of 13.

The flight dynamic model alongside the engine models and the new main rotor model performs a calculation step using an average time of **1.8 ms**, approximately 20% faster than the old one. Furthermore, the new model, having also activated the delay dynamic, has 10 more states. Although the higher model level and the greater number of states, the attention dedicated to the implementation and the design of the model has led to remarkable improvement.

5.1 Forward input test, 2.b.3 (i)

The first dynamic test is called in the normative[3] 2.b.3 (i). This test aims to evaluate the low airspeed handling qualities following a step control input on the longitudinal control. As reported in the legislation, it is specifically noted that off axis response must show correct trend. The longitudinal command applied in this test is a forward cyclic, hence pitch down, and it is represented in the first plot of figure 5.1. The initial trim conditions are shown in table 5.1: they are performed at a very low speed and the rates are practically zero. The helicopter is then in hovering flight out of ground effect. The static results can be also seen in the first seconds of the test before the happening of the step control input. The comparison is made with overplots of the three tests: the measured flight test data is shown in blue, the old model data in purple and the new model results in dashed green. First of all, it can be observed that the on-axis response with the command, the pitch angle and pitch angle rate trends are comparable to those measured in the flight tests, both in the initial instants and the long term response.

Although the old model presents an acceptable initial starting point, it responds in the mid-long term with trends that are not comparable with those measured by the helicopter. Eventually, the off-axis response of bank angle and roll rate shows trends comparable to those of the flight tests. The rates of the off-axis response are the ones to be noted to permit the validation of the model goodness.

Therefore, by observing the roll rate, it is possible to confirm a coherence in the short-medium term off-axis response. On the contrary, the off axis response of the old model is characterized by a trend that is not comparable with the one of the simulated data.

Parameter [UoM]	Reference	FSTD	MQTG
Mass Properties			
Gross Weight [kg]	2825.2	2825.2	2825.2
Fuel Weight [kg]	148.2	148.2	148.2
CG Longitudinal [mm]	4497	4497	4497
CG Lateral [mm]	-10	-9	-9
Moment of Inertia XX; XY; XZ [kgm^2]	0; 0; 0	2717; 37; -1694	2717; 37; -1694
Moment of Inertia YX; YY; YZ [kgm^2]	0; 0; 0	37; 11626; 17	37; 11626; 17
Moment of Inertia ZX; ZY; ZZ [kgm^2]	0; 0; 0	-1694; 17; 10196	-1694; 17; 10196
Environment Parameters			
Pressure Altitude [ft]	1470	1462.7	1462.7
OAT [degC]	21	21	21
Wind Direction [deg]	0	0	0
Wind Speed [kts]	0	0	0
Flight Parameters			
Airspeed [kts]	-0.2	2.5	2.5
Ground Speed [kts]	2.4	2.6	2.6
Vertical Velocity [ft/min]	75.9	70.9	70.8
Radar Altitude [ft]	283.2	1470.4	284.9
Rotor Speed [%]	102.7	102.7	102.7
Engine 1 Torque [%]	61	62.6	60.6
Engine 2 Torque [%]	61.2	62.6	60.6
Pitch Angle [deg]	4.6	4.2	4
Bank Angle [deg]	-1.7	-3.3	-3.2
Heading [deg]	250.2	249.9	249.9
Pitch Rate [deg/s]	-0.2	0	0
Roll Rate [deg/s]	0.4	0	0
Yaw Rate [deg/s]	0.1	0	0
X Body Acceleration [m/s^2]	-0.1	-0.1	-0.1
Y Body Acceleration [m/s^2]	0	-0.1	-0.1
Z Body Acceleration [m/s^2]	0	0	0
Longitudinal Cyclic Pos. [%]	62.7	52.9	53
Lateral Cyclic Pos. [%]	58.3	48.5	48.7
Pedals Pos. [%]	31.6	38.7	39.4
Collective Pos. [%]	54.5	43.3	42
Engine 1 Main Switch [-]	FLIGHT	FLIGHT	FLIGHT
Engine 2 Main Switch [-]	FLIGHT	FLIGHT	FLIGHT
AFCS State [-]	OFF	OFF	OFF
Training Mode [-]	OFF	OFF	OFF

Table 5.1. 2.b.3 (i) Initial test data

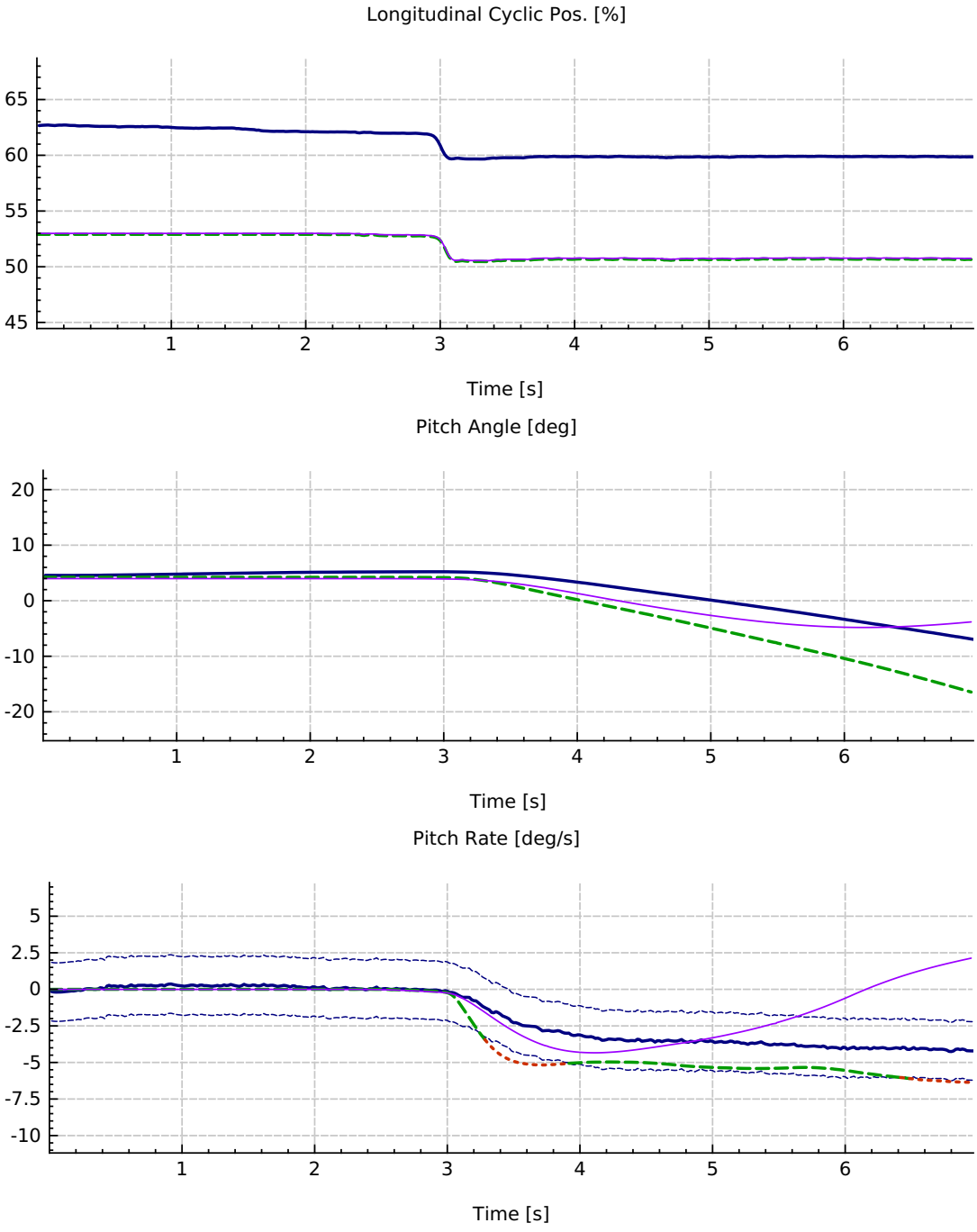
Longitudinal Cyclic Pos. [%]
65
60
55
50
45
1
2
3
4
5
6
Time [s]
Pitch Angle [deg]
20
10
0
-10
-20
1
2
3
4
5
6
Time [s]
Pitch Rate [deg/s]
5
2.5
0
-2.5
-5
-7.5
-10
1
2
3
4
5
6
Time [s]

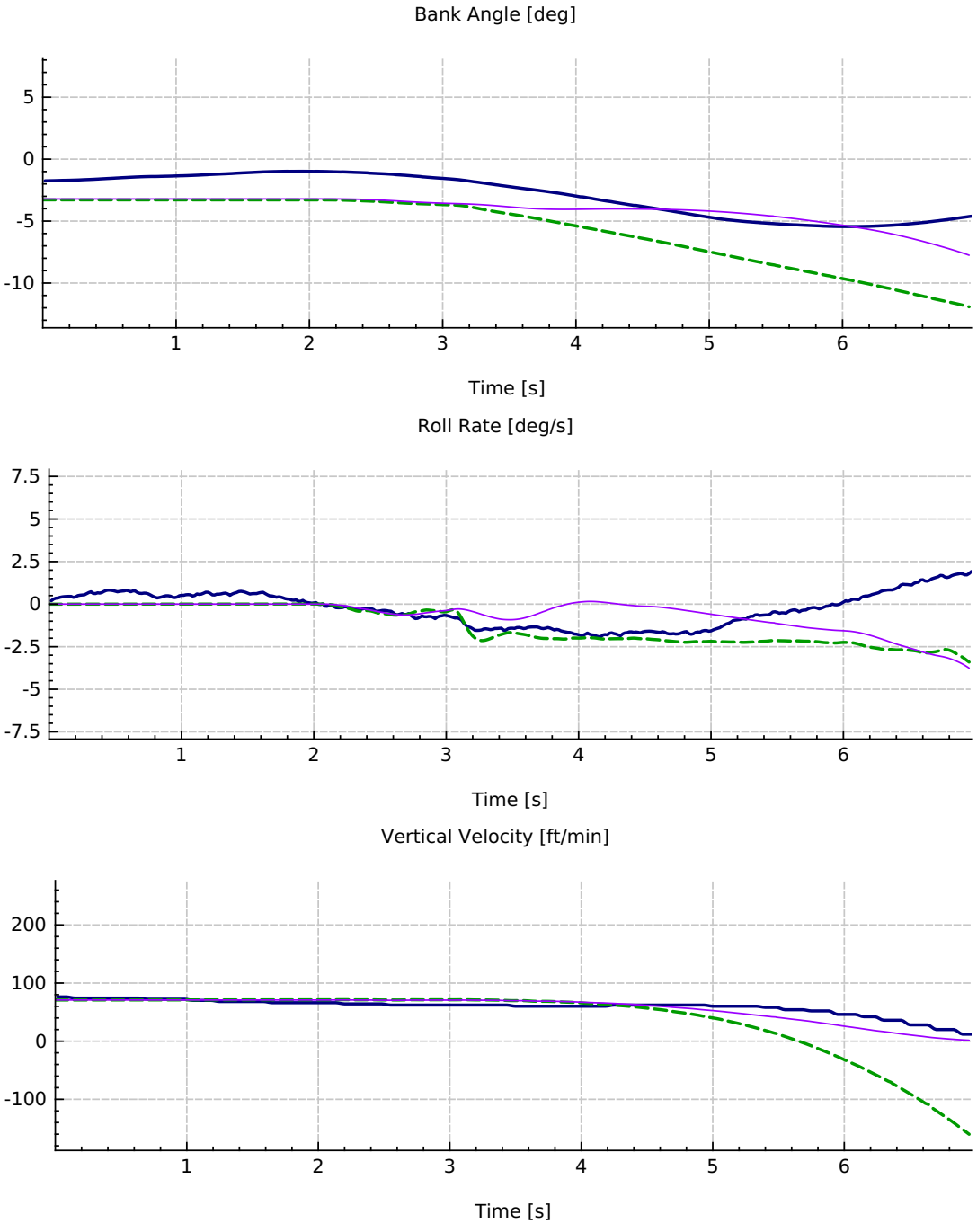
Bank Angle [deg]
5
0
-5
-10
1
2
3
4
5
6
Time [s]
Roll Rate [deg/s]
7.5
5
2.5
0
-2.5
-5
-7.5
1
2
3
4
5
6
Time [s]
Vertical Velocity [ft/min]
200
100
0
-100
1
2
3
4
5
6
Time [s]

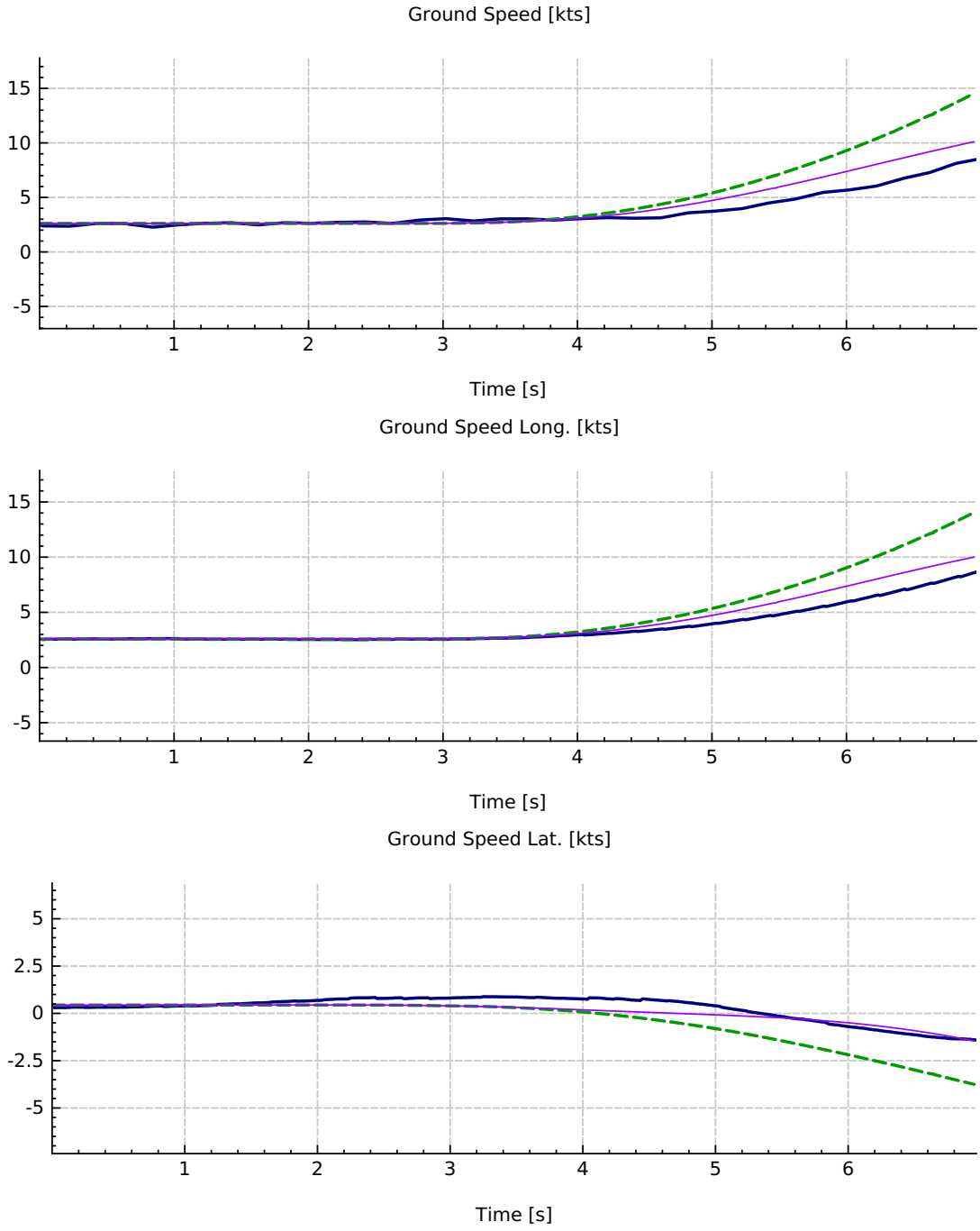

Figure 5.1. 2.b.3 (i) test results

5.2 Left input test, 2.b.3 (ii)

This dynamic test is called in the normative[3] 2.b.3 (ii). This test aims to evaluate the low airspeed handling qualities following a step control input on the lateral control. As reported in the legislation, it is specifically noted that the off-axis response must show correct trend, such as for the longitudinal control response test. The lateral command applied in this test is leftward cyclic, hence left roll, and it is represented in the first plot of figure 5.2. The initial trim conditions are shown in table 5.2: they are performed at a very low speed and the rates are practically zero. The helicopter is in hovering flight out of ground effect.

The on-axis response at the left command (shown in the bank angle and roll rate) shows trends comparable to those measured in the flight tests, both in the initial instants and in the long term response, as for the previous test. Also for this test, the old model response in the mid-long term has trends less comparable with those of the real aircraft.

Analysing the off-axis response by observing pitch angle and pitch rate overplots, it is more evident how the new model response is similar to the measured one. The old model test data, on the contrary, shows even an opposite off-axis response. It is possible to see that the off-axis response is coherent for both axis commands, in contrast with the old model.

Parameter [UoM]	Reference	FSTD	MQTG
Mass Properties			
Gross Weight [kg]	2825.2	2825.2	2825.2
Fuel Weight [kg]	148.2	148.2	148.2
CG Longitudinal [mm]	4497	4497	4497
CG Lateral [mm]	-10	-9	-9
Moment of Inertia XX; XY; XZ [kgm^2]	0; 0; 0	2717; 37; -1694	2717; 37; -1694
Moment of Inertia YX; YY; YZ [kgm^2]	0; 0; 0	37; 11626; 17	37; 11626; 17
Moment of Inertia ZX; ZY; ZZ [kgm^2]	0; 0; 0	-1694; 17; 10196	-1694; 17; 10196
Environment Parameters			
Pressure Altitude [ft]	1470	1462.7	1462.7
OAT [degC]	21	21	21
Wind Direction [deg]	0	0	0
Wind Speed [kts]	0	0	0
Flight Parameters			
Airspeed [kts]	-0.2	2.5	2.5
Ground Speed [kts]	2.4	2.6	2.6
Vertical Velocity [ft/min]	75.9	70.9	70.8
Radar Altitude [ft]	283.2	1470.4	284.9
Rotor Speed [%]	102.7	102.7	102.7
Engine 1 Torque [%]	61	62.6	60.6
Engine 2 Torque [%]	61.2	62.6	60.6
Pitch Angle [deg]	4.6	4.2	4
Bank Angle [deg]	-1.7	-3.3	-3.2
Heading [deg]	250.2	249.9	249.9
Pitch Rate [deg/s]	-0.2	0	0
Roll Rate [deg/s]	0.4	0	0
Yaw Rate [deg/s]	0.1	0	0
X Body Acceleration [m/s^2]	-0.1	-0.1	-0.1
Y Body Acceleration [m/s^2]	0	-0.1	-0.1
Z Body Acceleration [m/s^2]	0	0	0
Longitudinal Cyclic Pos. [%]	62.7	52.9	53
Lateral Cyclic Pos. [%]	58.3	48.5	48.7
Pedals Pos. [%]	31.6	38.7	39.4
Collective Pos. [%]	54.5	43.3	42
Engine 1 Main Switch [-]	FLIGHT	FLIGHT	FLIGHT
Engine 2 Main Switch [-]	FLIGHT	FLIGHT	FLIGHT
AFCS State [-]	OFF	OFF	OFF
Training Mode [-]	OFF	OFF	OFF

Table 5.2. 2.b.3 (ii) Initial test data

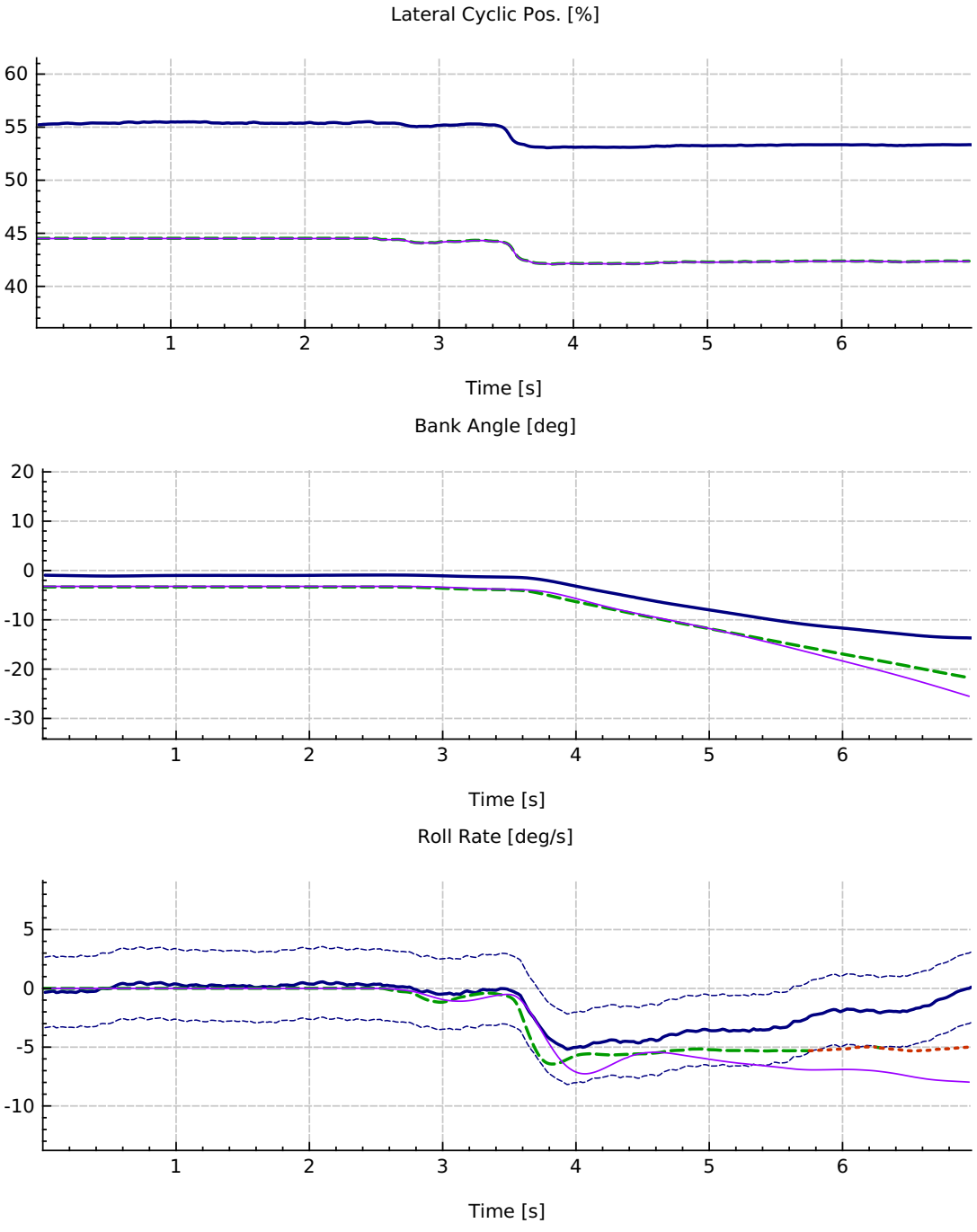
Lateral Cyclic Pos. [%]
60
55
50
45
40
1
2
3
4
5
6
Time [s]
Bank Angle [deg]
20
10
0
-10
-20
-30
1
2
3
4
5
6
Time [s]
Roll Rate [deg/s]
5
0
-5
-10
1
2
3
4
5
6
Time [s]

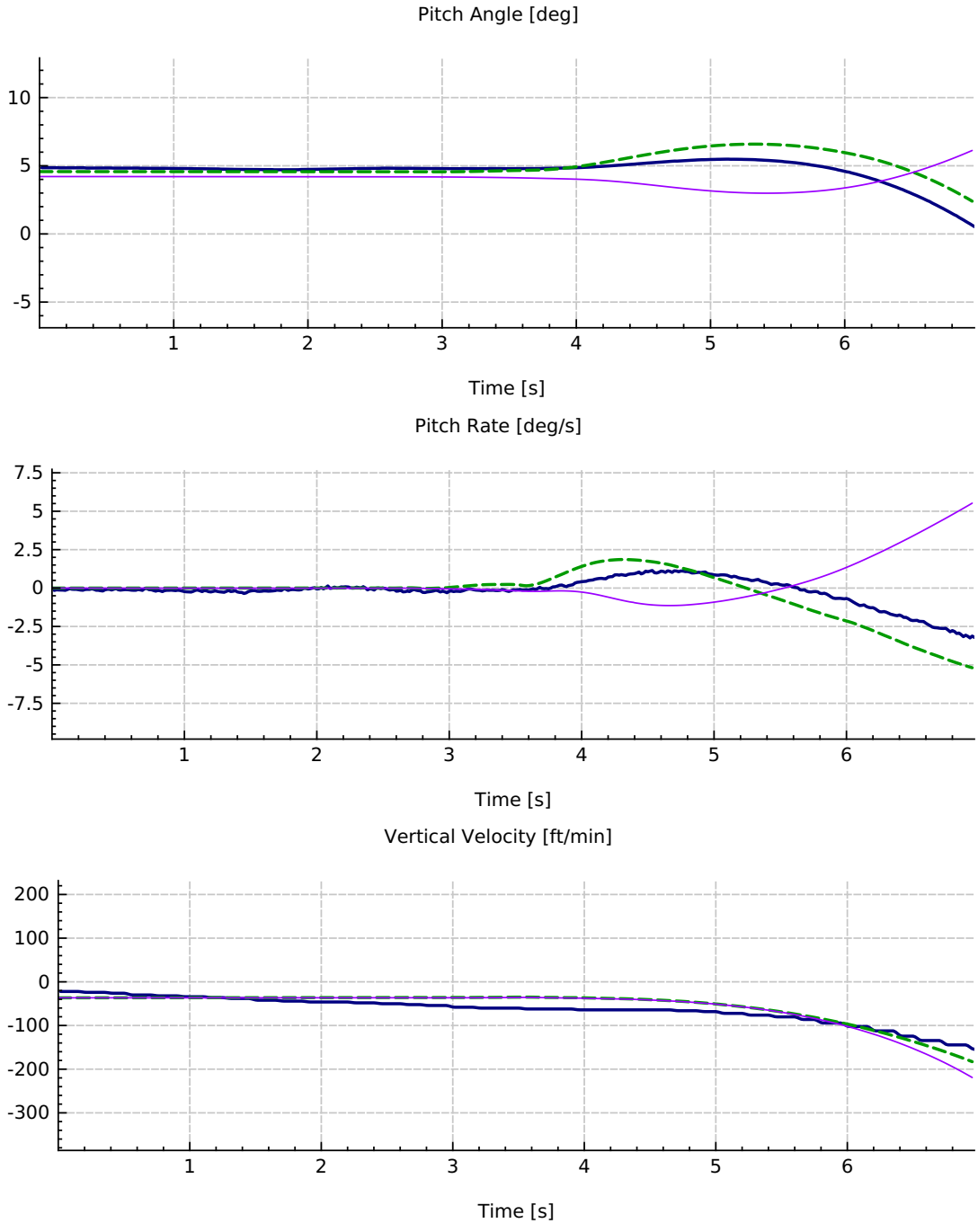
Pitch Angle [deg]
10
5
0
-5
1
2
3
4
5
6
Time [s]
Pitch Rate [deg/s]
7.5
5
2.5
0
-2.5
-5
-7.5
1
2
3
4
5
6
Time [s]
Vertical Velocity [ft/min]
200
100
0
-100
-200
-300
1
2
3
4
5
6
Time [s]

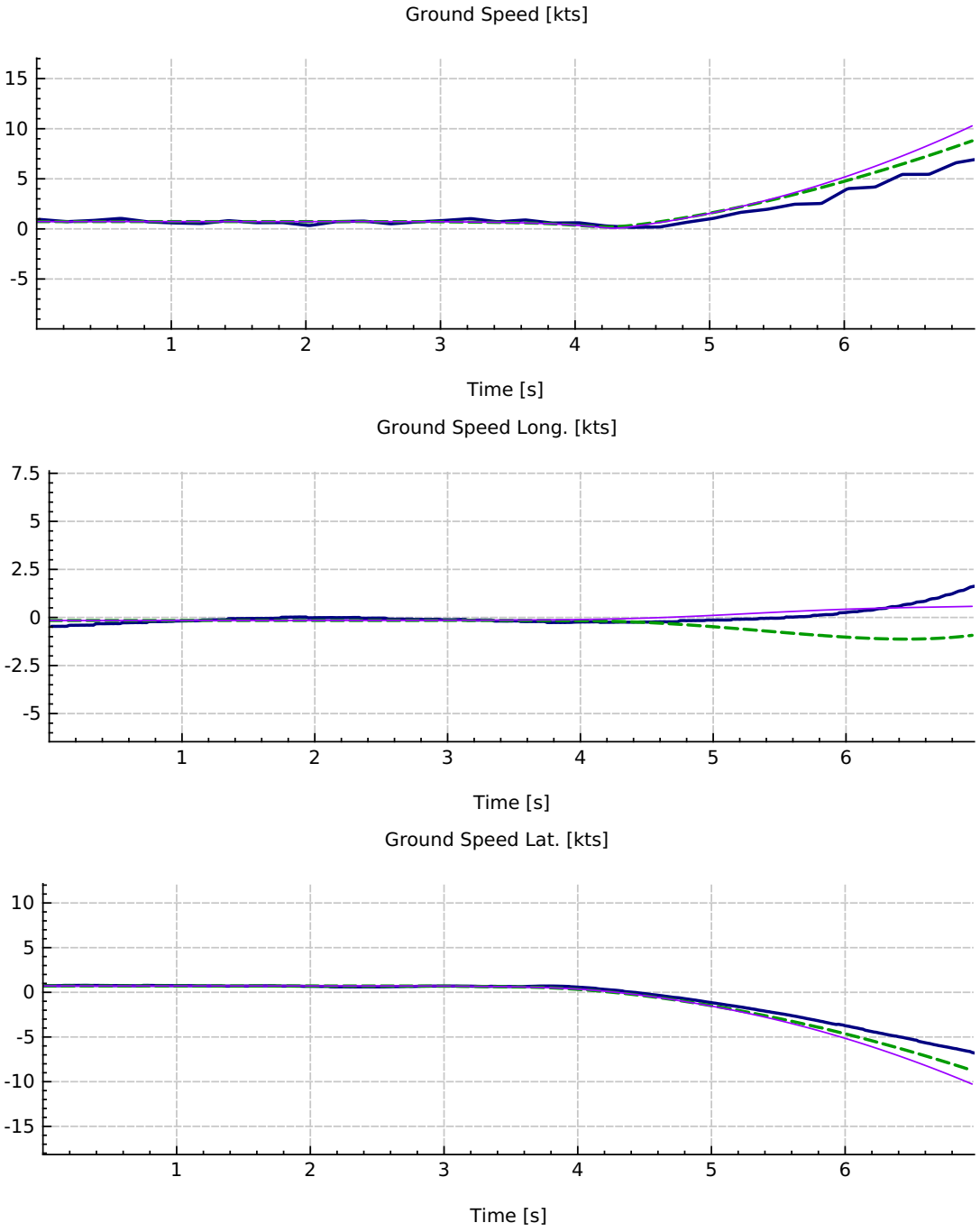

Figure 5.2. 2.b.3 (ii) test results

5.3 Model evolution

The future evolution of the model will be carried out to improve two properties in particular:

- **the level of generality**, to allow to simulate other similar helicopters, primarily through physical configuration;
- **the level of modelling complexity**, to increase the level of precision in the representation of physical phenomena.

The evolution of the model must in any case be carried out by recalling the purpose of the model, i.e. the simulation for training purpose. An advanced physical modeling consequently requires a large number of physical and geometric parameters peculiar of the aircraft. Furthermore, these parameters are often not available because they are under proprietary knowledge or because they are not easily measurable, requiring a further effort to estimate them.

However, a list of future improvement of the model has already been drawn up.
To improve the rotor head and blade kinematics, the model will be adjusted by adding some parameters and modifying some hypothesis:

- **Dynamic Twist** The local feathering angle of the blade section alongside the blade span is affected by aerodynamic loads that twist the rotor blades. A semi-empirical sub-model should be implemented as described in ref. [14]. The application of the dynamic twist will affect control position accuracy.
- **Blade Weight** Considering the blade weight will probably not alter significantly the flight dynamic. However, it could bring an important contribution to the rotor dynamic for the low rotational speeds. This should not be considered useful for the flight dynamic but only for some in-ground simulated procedures.
- **Pre-coning angle** The pre-coning angle is the reference coning angle (i.e. zero blade flap reference position); this should slightly affect the flight dynamic stability. It is a vastly used feature in rotor design.
- δ_3 **angle** This is the misalignment angle of the hinge pitch axis from the blade span axis. This feature creates the pitch-flap coupling and it is sometimes used in modern helicopters.
- **Non concentrated flap-lag hinges** The blade kinematic design usually has a non-concentrated flap and lag hinges. Even for bearingless helicopters, a sequence of equivalent hinges is observed in the elastic structures. This feature could affect the flight dynamic of the helicopter too.

Important evolution of the model will be performed form the aerodynamic point of view. By maintain the blade element method and a 2D aerodynamic, it is possible to make improvements by including some non-stationary effects:

- dynamic stall, for the receding blade element, would affect the aerodynamic loads;
- unsteady aerodynamic coefficients, extrapolated from the load hysteresis of the airfoil - this improvement should better estimate the near-stall loads of the pitching blade element.

To improve the inflow model, the Pitt/Peters model will be substituted with one of its evolution, the so called Peters-Ha [7]. As mentioned in ref. [6], this is an optimized version of the Pitt/Peters in both physical and implementation degrees. As a further evolution, a blade-inflow model with some 3D aerodynamic and a blade interacting wake could be taken into consideration.

One additional sub-model could be added to improve the modeling of the rotor: a **rotor head drag model**. The rotor head is usually a big and complex element: its rotation and its influence in the forward flight make it a non-negligible source of induced and parasite drag, affecting the overall performance of the aircraft. A semi-empirical model should be introduced to assess the overall contribution.

Most of the improvements proposed will be mathematically developed by using the already mentioned Matlab® symbolic script.

The paths that can be taken to improve the model are several. The purpose of this chapter is to provide general examples for some upgrades that can be easily implemented, taking advantage of the general and modular aspects of the design of the new model.

Chapter 6

Conclusions

In this thesis work, an already existing rotor model for a full flight simulator under development has been improved. Several problems affecting the existing rotor model have been addressed and solved, in particular the ones about instability and inconsistency of the off-axis response of the simulated flight dynamic. The work of this thesis has been divided in two parts.
Initially, flight dynamic instability issues were addressed. To do this, a coordinates transformation of the rotor states has been implemented. The transformation of the blade-flapping-states into multi-blade coordinates was carried out without modifying the implemented model simply by performing a code wrapping. By doing so, it was possible to efficiently solve the problem - the dynamic of the helicopter was then stable and comparable with the one of the real aircraft. The validation of the multi-blade coordinates was carried out by observing the static flight tests, the ones described by the normative for the formulation of the QTG document. By doing so, it was possible to highlight the gain acquired by using MB coordinates for numerical models.

In the second part of the thesis work, a new rotor model was developed. The old rotor model had inconsistencies in the dynamic response (in particular in the off-axis response) and it was developed and implemented in a not very rigorous way, also presenting various secondary problems. The new model was developed with the aim to be more mathematically rigorous, present a highest level of generality and configurability and be computationally performing. The new model also features a higher degree of physical modeling: in fact, the dynamic of the blade is described by the coupling of the flap and lead-lag degrees of freedom. The mathematical modeling is carried out rigorously and explained in detail in the thesis chapters. The formulations are based on dimensional equations. The implementation of the model was carried out paying particular attention to code performance and modularity with the aim of being able to easily make changes and improvements in the future. The results obtained with the new model showed a positive and promising outcome. Dynamic tests were conducted in hovering state, in order to avoid contribution from the fuselage and tail planes. The tests are applied and compared within the simulated models, the new and the old one, and the measured data of the flight tests. The validation of the model was qualitative, without the use of any tuning but the

realistic physical parameters of the simulated helicopter. Two tests of dynamic response in hovering to the step command are proposed: one on the longitudinal cyclic command with step forward and one with lateral cyclic command with step on the left. The model has been then validated: in fact, the inconsistency problems of the off-axis dynamic response have been solved. Progress has also been made from the point of view of computational performance, making the new model, albeit greater degrees of complexity, more efficient. To show the modularity of the architecture of the implemented model, there were also proposed a series of modifications and improvements that will be easily incorporated into the model in the near future.

In the end it was decided that this new rotor model will be used instead of the old one for the full flight simulator under development.

Appendix A

Frame of reference rotation

[11]. From the rotation angles defined by the vector:

$$r_{angles} = \begin{pmatrix} \phi & \theta & \psi \end{pmatrix} \tag{A.1}$$

Where: ϕ is the roll, θ is the pitch and ψ the yaw angle.
Individual rotations about the previous angles are performed with the following matrices.

$$R_{yaw} = \begin{bmatrix} \cos(\psi) & \sin(\psi) & 0 \\ -\sin(\psi) & \cos(\psi) & 0 \\ 0 & 0 & 1 \end{bmatrix} \tag{A.2}$$

$$R_{pitch} = \begin{bmatrix} \cos(\psi) & \sin(\psi) & 0 \\ -\sin(\psi) & \cos(\psi) & 0 \\ 0 & 0 & 1 \end{bmatrix} \tag{A.3}$$

$$R_{roll} = \begin{bmatrix} 1 & 0 & 0 \\ 0 & \cos(\phi) & \sin(\phi) \\ 0 & -\sin(\phi) & \cos(\phi) \end{bmatrix} \tag{A.4}$$

To compose the complete rotation with the correct order the following relation is used:

$$R_{total} = R_{yaw} R_{pitch} R_{roll}. \tag{A.5}$$

That gives the total rotation matrix:

$$R_{total} = \begin{bmatrix} \cos(\psi)\cos(\theta) & \cos(\theta)\sin(\psi) & -\sin(\theta) \\ \cos(\psi)\sin(\phi)\sin(\theta) - \cos(\phi)\sin(\psi) & \cos(\phi)\cos(\psi) + \sin(\phi)\sin(\psi)\sin(\theta) & \cos(\theta)\sin(\phi) \\ \sin(\phi)\sin(\psi) + \cos(\phi)\cos(\psi)\sin(\theta) & \cos(\phi)\sin(\psi)\sin(\theta) - \cos(\psi)\sin(\phi) & \cos(\phi)\cos(\theta) \end{bmatrix} \tag{A.6}$$

Bibliography

[1] Bramwell A.R.S. *Bramwell's helicopter dynamics*. American Institute of Aeronautics and Astronautics, 2001.

[2] Inc. Advanced Rotorcraft Technology. *FLIGHTLAB Theory Manual Volume One*.

[3] European Aviation Safety Agency. *Certification Specifications for Helicopter Flight SimulationTraining Devices CS-FSTD(H) initial Issue*. 2012.

[4] G. Bir. «Multiblade Coordinate Transformation and Its Application to Wind Turbine Analysis». In: (2008).

[5] et al Bir G. Chopra I. «University of Maryland Advanced Rotor Code (UMARC) Theory Manual, tecnical report UM-AERO 94-18». In: ().

[6] Robert T. N. Chen. «A Survey of Nonuniform Inflow Models for Rotorcraft Flight Dynamics and Control Applications». In: (1989).

[7] D. A. HaQuang N. Peters. «Technical Note: Dynamic Inflow for Practical Applications». In: (1988).

[8] J.J. Howlet. «UH-60A Black Hawk Engineering Simulation Program: Volume I - Mathematical Model». In: (1981).

[9] W. Johnson. *Helicopter Theory*. Princeton University Press, New Jersey.

[10] MathWorks. *MATLAB Documentation Center*.

[11] Arra Michele. *L'elicottero*. Hoepli.

[12] Gareth D. Padfield. *HELICOPTER FLIGHT DYNAMICS The Theory and Application of Flying Qualities and Simulation Modelling, second edition*. Blackwell Publishing, 2007.

[13] D. A. Pitt D. M. Peters. «Theoretical Prediction of Dynamic Inflow Derivatives». In: (1981).

[14] A. Torasso. «Low-order models and numerical techniques for the analysis of rotorcraft flight mechanics». In: (2012).

Ringraziamenti

Vorrei ringraziare in primo luogo il Professor Giorgio Guglieri che, oltre ad avermi trovato questo lavoro di tesi, con le sue lezioni ha contribuito in maniera fondamentale ad alimentare la mia passione per lo studio dell'ala rotante.

Un grazie particolare va a Matteo, che con la sua passione, conoscienza e pazienza, mi ha seguito in questo lavoro, dandomi un aiuto fondamentale e insegnandomi moltissimo, non solo in ambito tecnico. Vorrei ringraziare inoltre la TXT e tutto il team del progetto, pichè mi hanno permesso di svolgere un lavoro così interessante e stimolante, sarò molto felice di continuare a lavorare con voi!

Un ringraziamento speciale va ai miei genitori e Gina che mi hanno supportato e sopportato e sempre stimolato nell'avere curiosità e initeressi, che hanno sempre creduto nelle mie passioni e che mi hanno aiutato sempre ad affrontare serenamente questo, alle volte difficile, percorso di studi.

Un grazie speciale va a Cecilia che c'è stata in ogni momento, per ogni cosa... Aiutandomi anche nella stesura di questo lavoro. Questa volta ti porto al mare io!

Per concludere vorrei ringraziare tutti i miei amici, con cui ho condiviso nei più svariati modi, passioni, progetti, invenzioni, avventure, voli, dubbi, vino, merende e pasti abbondanti.